This document has been made public in Feb, 2009. This document appears to be non final revision. This document is proved without redaction or censorship. However it is not guaranteed this is the document submitted as it may not be.

Documentation

Further documentation is available on **instructables.com**

- http://www.instructables.com/id/%5BVideo%5D-Large-Scale-Mold-Making---Part-I/
- http://www.instructables.com/id/%5BVideo%5D-Large-Scale-Mold-Making---Making-the-Negat/
- http://www.instructables.com/id/%5BVideo%5D-Part-Making/
- http://www.instructables.com/id/Aerodynamic-Wheel-Disks---For-your-Bike/
- http://www.instructables.com/id/%5BVideo%5D-Mixing-Polyester-Resin/

Noted Issues

The vehicle exhibits a second vibration mode oscillation between the frame and fairing. This oscillation translates to the steering and is detrimental to steering and acceleration. This issue was resolved in 2008 by adding a mounting point in the front of the vehicle which stabilized the mass forward of the previously forward mounting points. Heed this error and make sure your noses either have a low mass or are affixed to your frame.

Shallow windscreen angle causes visibility issues due to optics. Especially when facing the sun.

Yes, those are submerged NACA ducts pointing backwards. Yes, we know that's not how they work. We had a mold, it's very easy to vacuum form a few extras. The design called for an exit hole – at that point on the fairing, it doesn't really matter how it gets out.

CoreMat is not an optimal core for this application – it's heavy and will eat resin. Use sparingly CoreMat where compression strength is needed. CoreMat should not carry a load – CoreMat is weaker than the resin (meaning the resin caries the load rather than the fiber).

Coverage

At the 2007 ASME HPV, east coast, this vehicle won 2nd in design, 4th in Sprint, 6th in Endurance and 3rd overall.

This vehicle made an appearance at the 2007 Bay Area Maker Faire at the San Mateo Fairgrounds in California thanks to a donation of booth space by instructables.com

Custodian

Please direct questions, comments, etc. to **robot@knights.ucf.edu** (As a robot, he feels no human emotion – which makes him sad)

University of Central florida
Human Powered Vehicle

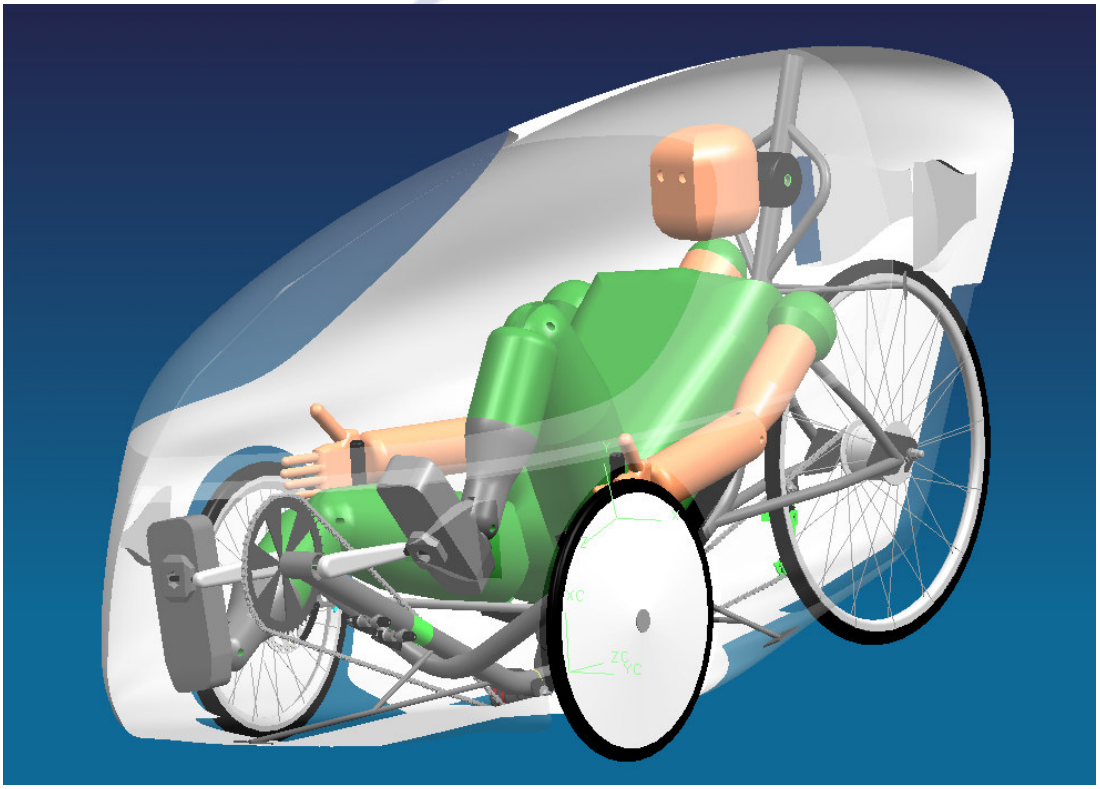

Engineered by:

Frame Team
Ashley Girdich
Luis Gonzalez
Matt Moten
Ori Raz-Russo

Fairing Team
Judy Deering
Lisa Johnson
Emilio Rivera

April 10, 2007

Table of Contents

Abstract

A well designed human powered vehicle involves planning, analyzing and innovation. Rules, regulations and customer specifications must be taken in the written form and transformed into a design and a then a final physical product. For this design challenge, a vehicle must meet the requirements of using only human power to transport a person to a desired destination. This year's team from the University of Central Florida has accepted the challenge and designed a vehicle with speed, innovation and safety in mind.

The process began by gathering all of the design parameters and regulations to develop goals for the team and the design. Two distinctive groups were formed, one to design the frame and one to design the fairing. Each team developed goals and design requirements that met the specifications provided by ASME. Both groups began a configuration design process that involved extensive research on the components involved for both the frame and the fairing. The team found that a three-wheeled tadpole, rear wheel driven design was the safest design to pursue and that a completely enclosed fairing with a ventilation system was the most aerodynamic solution.

Through research on brakes and gearing systems, the frame is equipped with hydraulic brakes and an internal gear system on the rear hub. The material used for the frame ranges from AISI 4130 Chromoly steel to 6061-T6 Aluminum. Each material was carefully selected with the strength and weight kept as main parameters followed by manufacturability. Special design features of the frame include an Ackerman steering geometry, and an idler wheel to reduce the number of contact points for the chain route. Regarding human size, there is not a one-size-fits-all vehicle, which is very important to design around. This year's team designed the vehicle with this in mind and produced a vehicle that can meet the needs of the smaller and larger riders through an extendable boom. To ensure stability of the vehicle, the center of gravity is a mere 11.75 inches off of the ground.

The fairing is designed around aerodynamic principles to ensure that the vehicle is as aerodynamic as possible with the constraints set by the frame. The ground clearance of the vehicle is designed to be a low 3.25 inches from the ground. As the competition occurs in sunny, humid and hot Florida, a ventilation system involving NACA ducts is incorporated into the design of the vehicle. Through examination and testing of materials, an S-glass fiberglass fairing is created with Core-mat material placed strategically for strengthening of the vehicle in potentially weak areas.

To verify the design of the team and the efforts put forth by the members, computer software is employed to put the design to the test. UGS Nx3 engineering based software is utilized to model the frame and apply various loads experienced through braking and rollover scenarios. Through analysis of these scenarios and the data they provided, the frame was designed with a 3:1 safety ratio. Through the use of COSMOS FloWorks and the Computational Fluid Dynamic's package, the model of the fairing was optimized for a low coefficient of drag of 0.25. Further testing ensued on the fairing through wind tunnel testing that analyzed the pressure gradient surrounding the vehicle. All of the results of the tests described enabled further tuning of the vehicle to the most optimal design which then in turn provided the blueprints for the physical product.

Vehicle Design Description

Initial Design criteria

The target goal for UCF's HPV team is to design a vehicle that is lightweight, aerodynamic, safe, and enjoyable to ride. The vehicle must be able to adapt to its surrounding environment as well as the rider. The design of the vehicle began by listing all the customer requirements and weighing their importance with a House of Quality matrix. The customer's requirements were gathered from documentation as well as verbal presentations from UCF's ASME chapter members, UCF's MMAE facility, and ASME's competition regulations. Based on this analysis, the safety of the vehicle was the biggest design parameter followed by aerodynamics, over all vehicle weight, and maximum speed capabilities. All of ASME's safety requirements were considered as a must have design feature. The vehicle must stop within 20ft traveling at a rate of 15mph, incorporate rollover protection into the design, and have steering capabilities that allow the vehicle to have a minimum turning radius of 25ft. Next, engineering target goals and guidelines were constructed to optimize the design of the vehicle. For example, the maximum target speed of the vehicle was set to be 43mph. These goals were based on previous UCF's HPV production as well as other competing school's results form the 2006 East Coast HPV challenge, see Table 2.1 for target goal.

Topic	Units	2006-2007 Target	2005-2006 Results
Top Speed	mph	40-43	36
Overall Weight	Pounds(lbf)	Under 60	72
Drag Coefficient	Unit less	0.4 - 0.2	0.39
Length/Width/Height	Inches(in)	Under 96/36/45	94/29/54
Rider Exchange Time	Seconds(s)	Under 25	63
Ground Clearance	Inches(in)	3 - 5	7.5

Table 2. 1 Target Goals for UCF's 2006-2007 HPV

The best possible vehicle configuration was found by utilizing a Kepner Tregoe Decision Analysis (KTDA) used for concept weighing analysis. Several different vehicle configurations were analyzed to find the best possible design solution. For example, two, three, and four wheeled designs were weighed and analyzed based on engineering knowledge, practicality, and originality, see Figure 2.1 for initial design drawings. From past year's experience, delta tricycles were found to be very unsafe during high speed turning scenarios; therefore, this type of vehicle was eliminated due to safety concerns. Four wheeled vehicles were also eliminated due to unpractical weight and production cost issues. Finally, the best possible solution was selected to be a three wheeled tadpole recumbent, rear wheel drive, fully enclosed streamlined vehicle.

The tadpole design is a very safe and stable vehicle configuration. This design will help minimize the rider exchange time during the endurance race as well as provide a safe and stable riding platform for any rider. In general, three wheeled vehicles are heavier and slower than a two wheeled design. However, three wheeled vehicles are rider friendly, comfortable to ride, and very safe to maneuver at various speeds. The recumbent riding position will provide a low center of gravity that will allow the vehicle to turn at a high rate of speed while minimizing a roll over scenario. It will also allow the fairing's frontal area to be minimized which correlates into low drag losses. A rear wheel driven drive train was selected due to its design practicality based on the overall vehicle configuration.

Human Fitting

The modeling of the vehicle's configuration began by building a wooden mock fitting test stand that allowed all the possible riders to be accurately fitted and measured relative to the best recumbent riding position. Ergonomic bicycle studies showed that the human body can generate maximum power by allowing the riders knee to be positioned inline with the ball of his or her foot at the beginning of the power stroke, see Figure 2.2 for reference. This will allow the rider to utilize the larger muscles in his or her legs during the power stroke and maximize the acceleration potential of the vehicle **(Stanek, 3**). The fitting test

stand was designed to be adjustable depending on the rider's shape and size. For example, the neck and back angles could be adjusted until the rider's visibility and comfort levels were satisfied. From this fitting test, the rider's back and neck angle, bottom bracket height and over all head height relative to the ground were recorded and analyzed for positioning trends. Rider body dimensions were taken for human modeling purposes that will aid in the accurate modeling of the fairing relative to the frame's design. For example, each rider's shoulder width, waist width, arm length, leg length, X-Seam distance, shoe size, and head dimensions were measured, see Figure 2.2 for body dimension locations. Additionally, the rider's visibility was maximized while finding the best ergonomic fitting solution. This was achieved by allowing each rider

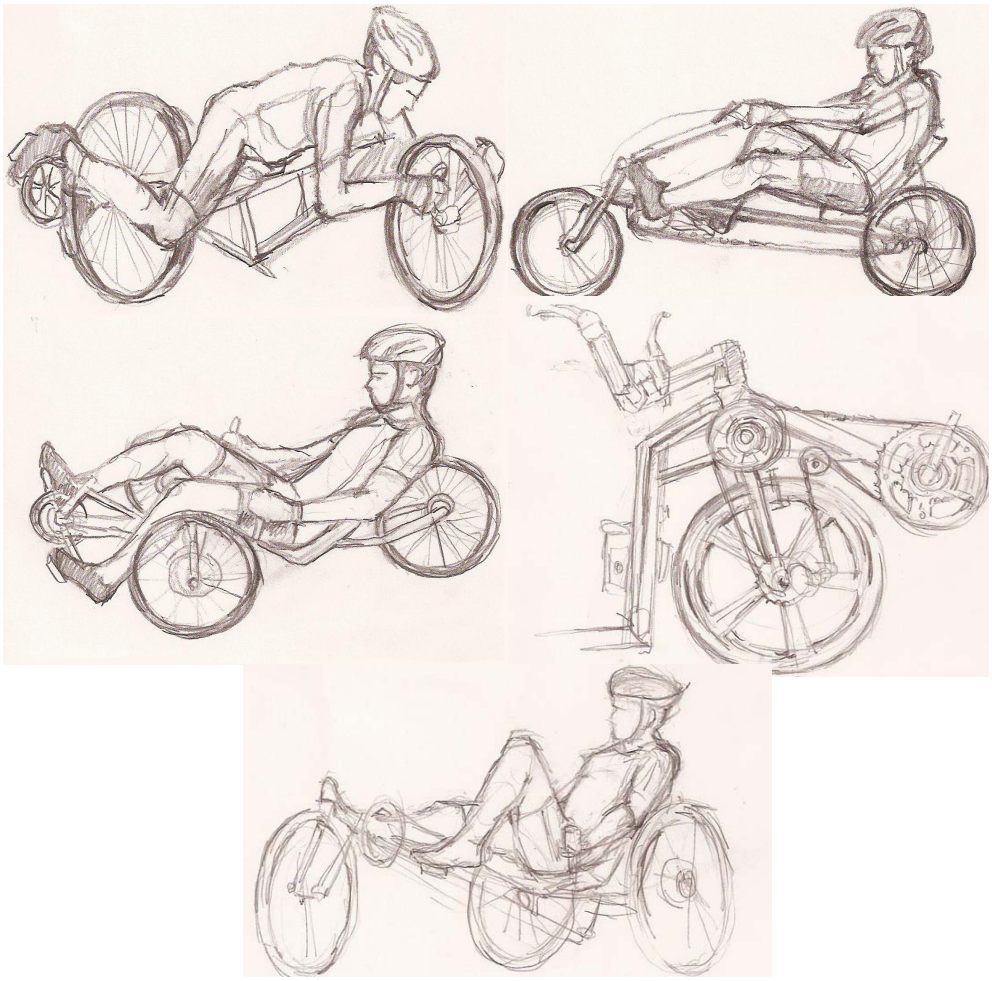

Figure 2.1 Initial Design Consideration Drawings (Drawn by Ori Raz-Russo)

to see over his or her knees at its maximum height position. This safety feature was incorporated early in the design process to maximize the safety potential of the overall vehicle design. From this data, the bottom bracket positioning was noted to be very staggered depending on the shape and size of the rider legs. All the fitting data was drafted in a 2D AutoCAD drawing to find all possible frame configurations that fit best with the rider's body dimensions. Finally, the boom angle was selected to be 26^0 from the horizontal, while the back and neck angles were selected to be 30^0 and 70^0 respectively. This allows the design to have a minimum ground clearance of 3.25 inches which is below the initial target design goal.

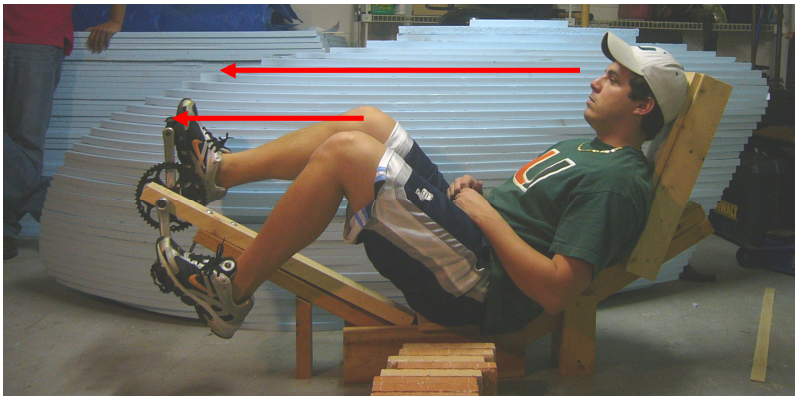
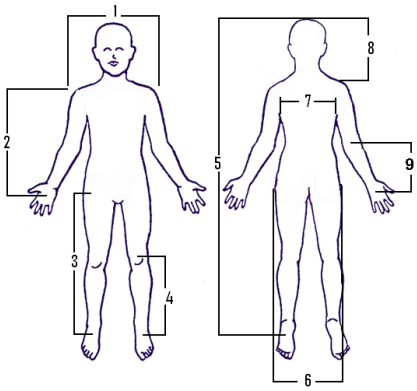

Figure 2.2 Human Fitting Mock Test Stand and Body Measurements

Braking

The Avid Juicy 7 hydraulic disc brake system was chosen due to its ability to meet the ASME braking requirement as well as having the ability to adjust braking power on the fly. There are two major requirements that the brake system must satisfy. First of those requirements is set by ASME and it requires that the HPV come to a stop from 15 mph in a distance of 20 feet or less. In order to meet the first requirement, it was decided to use disk brakes. While the ASME requirement is simple to satisfy, a shorter stopping distance is desired for the sake of safety. The other requirement is that the vehicle comes to a stop within 100 meters of the sprint competition end line. The vehicle will be doing approximately 30 to 40 miles per hour at the end of the sprint; however 100 meters (~330 feet) is a large stopping distance, making this requirement not as difficult to achieve as the initial ASME requirement. According to calculations, a force of at least 102lbf should be applied to stop the vehicle within 20 feet.

In order to calculate the amount of force required to stop the HPV in accordance with the ASME requirement, the amount of kinetic energy lost while the vehicle comes to a stop must be found. The equation for finding the kinetic energy can be found in the Braking Forces Calculation Sheet. The mass, velocity and distance are required in order to find the force.

The combined braking forces were found to be 102 lbf with the heaviest rider, and 49 lbf with the lightest rider. In order to prove that the hydraulic disk braking system is capable of meeting the ASME requirement, it must shown that they can produce at least 103 lbf of braking force. To do this, the frictional force generated by the brake pads opposing the rotor must be calculated. To find these forces various manipulations of the kinetic energy equation were used.

The force of the brake system's clamp was found to be approximately 200 lbf when the brake lever was depressed at a maximum of 20 lbf. In order to accurately gauge the force of friction, a range of values was used because the coefficients of friction from pads vary according to temperature. With a coefficient of friction of .3, see Table 2.2 for reference, the two front wheels of the HPV could produce a combined braking force of 120 lbf, which overcomes the required 103 lbf calculated from ASME's requirements. Theoretically the brakes will be able to produce well over 200 lbf, although so much force being applied would result in the tires locking up on the asphalt. In order to stop the vehicle within 20 feet from 15 mph, a braking force of over 102lbf is required. However, a force of over 200 pounds could cause wheel lock, which is why the design limitation is between 102 and 200 pounds. Because the sprint braking requirement is 330 feet, much less braking force is required to stop the vehicle, even from a max velocity of 40 mph. The minimum braking force was found to be approximately 50 lbf. Once again the design limitation ends at 200 pounds to avoid tire wear.

Coefficient Of Friction (Pads)	Force of Friction per tire
.3	60 lbf
.4	80 lbf
.5	100 lbf
.6	120 lbf

Table 2.2 Coefficient of Friction on Tires

Gearing

Figure 2.3 shows the breakdown of crank selection calculations that were preformed to find the best gear ratios. In order to perform these calculations, the rear wheels circumference, diameter, internal hub's ratios, and sprocket sizes were required. From these calculations, it is recommended to have the vehicle equipped with two different types of crank sprockets, one for each event. For the endurance race the maximum desired sustained speed is set at 25 mph which results in a crack sprocket size of 32 teeth or higher. For the sprint, a maximum speed of 40 mph is desired which correlates to a crank equipped with 44 teeth or higher. The final recommendation is not only based on our calculated values but the availability of the component and its room for human progression. The final recommendations were selected to be a 53 tooth sprocket for the sprint and a 33 tooth sprocket for the endurance race. These selections will give the riders some room for improvement in case he or she runs out of gears during one of the events. To save on the complexity of the design and component construction, these gears will be manually changed before the event will start. To keep the weight down in this very heavy but curtail component, the crank will be constructed out of carbon fiber as apposed to standard aluminum.

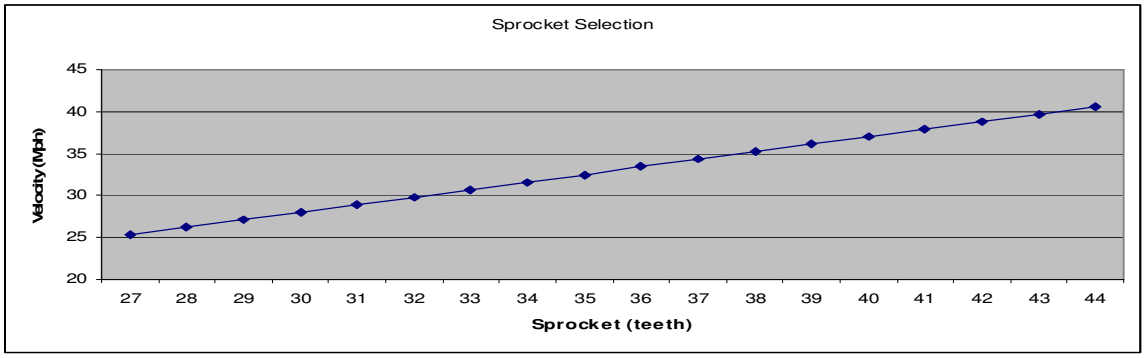

Figure 2.3 Sprocket Selection Table with Corresponding Speeds

Material Selection (Frame)

The selection of the frame material is important relative to the weight, strength, safety, manufacturing, and cost of the vehicle. All these areas weighed upon the best types of materials that could be selected. In order to choose the best possible material basic requirements needed to be considered. For example, the material for the frame should not be brittle or very ductile. In Figure 2.4b, the lower limit for the fracture strength of the material is set to 15 MPa*$m^{1/2}$ which eliminates all ceramics. In Figure 2.4a, the index that is being maximized is for tubes in bending (diagonal line) and the lowest stress that the vehicle can withstand is estimated to be 200 MPa (from Iterative FEA analysis). This eliminates foams, polymers and natural materials such as wood. The main groups of materials left for consideration are composites and metals. Table 2.3 lists the properties of the materials that were initially considered in the frame's material selection process. Based on properties alone, carbon fiber would be the material of choice for this application; however, manufacturing and costs must also be considered in this selection process. Due to carbon fiber's high cost and low market availability, it was eliminated from being a possible solution. The next best material is titanium; however, titanium is also very expensive and difficult to manufacture due to welding limitations. Finally, aluminum and steel were selected as the top two main materials in the frames design and construction. The selection of the proper alloy of each material was based on the weld-ability of that particular alloy. In general, aluminum is more difficult to weld, due to its low melting temperature, compared to steel. Some aluminum alloys need to be heat treated after welding due to the gross loss in strength in the material. This is due to the rapid heating of the material in localized locations that brings the alloy above its critical temperature (Callister, Jr.4). Heat treatments are also very expensive and time consuming for such a design project as this. Based on this initial material manufacturing consideration, AISI 4130 normalized steel (Chrome-Moly Steel) was selected for the frame's main component material selection. This particular steel alloy has a high strength to density ratio. This material selection is also a very safe solution and does not require heat treatments after manufacturing. Aluminum alloys were not completely ruled out for other possible applications in the design. Aluminum will be used on parts that do

not require a lot of welding or machining. An aluminum alloy such as 5052-H32 and 6061-T6 will be incorporated into specific components that require certain material properties.

Ranking	Material	Density (ρ)	Elastic Mod (E)
1	Carbon Fiber	0.065 lb/in³	34,800 ksi
2	Titanium (6-4)	0.16 lb/in³	15,200 – 17,400 ksi
3	Steel (AISI 4130)	0.284 lb/in³	29,700 ksi
4	Aluminum(6061-T6)	0.097 lb/in³	10,000 ksi
5	Aluminum(5052-H32)	0.097 lb/in³	10,200 ksi

Table 2.2 Material Properties for all Materials Considered
Material Properties (Callister,Jr.4)

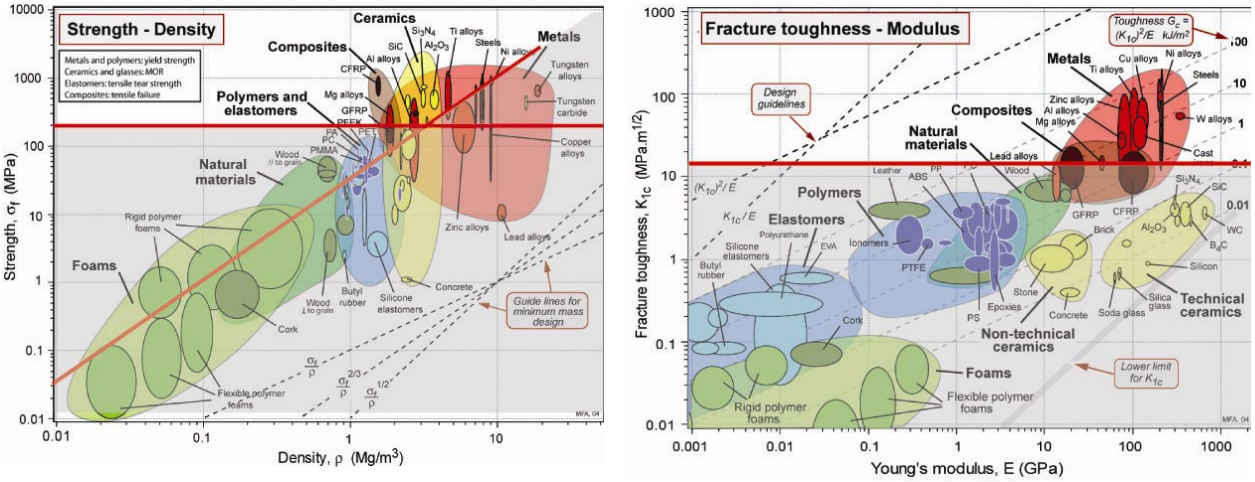

Figure 2.3a, b Material Selection Charts

Frame Design Features

The standard Ackerman steering configuration was selected to give the tadpole design the most efficient turning motion. The design of the steering system began with the selection of two 18 inch wheels from SunRim and two Schwalbe Stelvio tires. The small wheel diameter selection will help minimize the vehicle's component weight, and it will help reduce the aerodynamic drag of the vehicle by minimizing the wheel well cutouts in the fairing. This wheel size led to a caster angle selection of 10^0. This gives the steering system the optimal caster trail length of approximately 40mm. Unfortunately this design parameter was missed judged in last years HPV design. An extreme caster angel of 16^0 was incorporated in the steering geometry which led to extreme wheel flopping effects during riding. For this reason, each steering parameter was researched extensively. For example, the optimal caster angle was based on an average array of current production HPV's that are on the market, such as Greenspeed's GTO, GTX, and GTX models as well as BIGCAT's speed, trail, and 700 series trikes. Each of these vehicles's steering geometry parameter was measured in person and tabulated for analysis. It was noted that each vehicle that was measured showed similar steering parameters based on the vehicles desired steering outputs. For example, it is sometimes desired to steer a vehicle by the use of the brakes (brake steering); however, this steering parameter is not desired in UCF's steering geometry design. Therefore, the center point steering angle was selected to be approximately 23^0 based on this design specification of a non-brake steering vehicle. This specific angle projects a line that will intersect the outside face of the front wheels, This design parameter will also help prevent bump steering by redirecting the impulse forces caused by a road hazards (bumps, pot holes, and rocks…) in a direction away from the steering axel. In theory, the proper selection of these parameters will allow the vehicle to travel at any speed and come to a complete and safe stop by only using

one side of the braking system. This safety feature is evident in a down hill high speed scenario. If for some reason one side of the braking system would have failed the rider could safely stop the vehicle without losing control.

To incorporate these steering parameters into the design, two BIGCAT HPV raw stock spindles were used, see Figure 2.4 Detail D. These spindles were purchased based on the manufacturing expense of this part and satisfaction of UCF's steering specifications. The spindles are equipped with two quick release axles that will allow for quick tire repair if necessary, see Figure 2.4 for reference. The handlebars on the steering system are made from two of the same parts for easy manufacturability. Two standard bicycle handlebar-mounting rods make up the assembly which can be arranged in many different configurations depending on the event or the rider's preferences, see Figure 2.4 Detail E. For example, the handlebars can be configured to be insensitive for the sprint race by moving the bars as far back as possible and visa-versa for the endurance race. Next, the human fitting measurements were used to calculate the minimum wheel track distance needed to allow the rider to enter and exit the vehicle efficiently without clashing with the steering components. The selection of this parameter will dictate the overall width of the fairing and the aerodynamic capabilities of the vehicle. For this reason it is imperative to minimize this design parameter. The wheel track was selected to be 33 inches while the wheelbase was set to 44 inches. The steering axle that connects the steering assembly to the frame is made from 0.065 inch thick 4130 normalized steel. The wall thickness of the axle is noted to be larger than the frame's backbone thickness (0.049") because this component will be under larger loads during braking and turning scenarios.

Finally, the steering system triangle was drawn and the push rod placement was selected to complete the four bar mechanism of the Ackerman steering system. This four bar mechanism is the key component to the Ackerman steering geometry, see Figure 2.4 Detail E for reference. This will allow the inside wheel to turn at a greater angle than the outside wheel to help minimize tire scrub during turning, see Figure 2.4 for reference. The pushrod assembly consists of two aluminum rod-ends that are connected by an aluminum push-rod to minimize the overall weight of the component. It was noted that the forces in the steering push-rod were minor during the worst possible turning scenario; therefore, each rod-end is capable of handling 30lbf rather than a heavier steel assembly that can handle up to 80 lbf. The assembly is manufactured by using both right and left hand standard threads (1/4-28NTPS) to allow for easy adjustment of the steering system. For example, the push rod assembly can be fastened to the steering spindles and adjusted by simply twisting the push-rod depending on the desired outcome. This will in effect move each rod-end in opposite directions and push or pull the front wheels into proper alignment. Two jam nuts are fitted on each side of the assembly to lock the rod-ends into place. The thread count (28TPSI instead of a standard 20TPSI) was also selected to allow for an insensitive adjustment feature in the assembly**,** see Figure 2.4 for reference.

The human fitting analysis showed a wide range of body dimensions between each rider. The largest rider weighed 200lbf at a height of 6ft while the shortest rider weighed 81lbf at 4ft 11in. To allow for all of the members of this year team to be able to ride the HPV, a telescoping boom is implemented in the design. This boom is constructed of 6061-T6 Aluminum to reduce the weight of the component. Limited welding to the boom sleeve was done during manufacturing so no heat treatments were necessary on this particular part. Initially, the boom was configured to slide inside the frame's inner diameter; however, engineering knowledge of stress in metals dictated that a larger cross-sectional area will result in a larger moment of inertia and thus a smaller maximum stress in the boom, see Equation 2.1. In order to increase the amount of stress that the part can withhold, the connection of the boom to the frame is in the form of a male-female connection. This type of connection increases the moment of inertia of the cross-section, which decreases the maximum stress in the component. This design consideration was derived from the observation that a large force is going to be applied to the bottom bracket during pedaling in both the sprint and endurance competition.

Equation 2.1 Maximum Stress in a Cantilever Beam $$\sigma = \frac{Mc}{I}$$

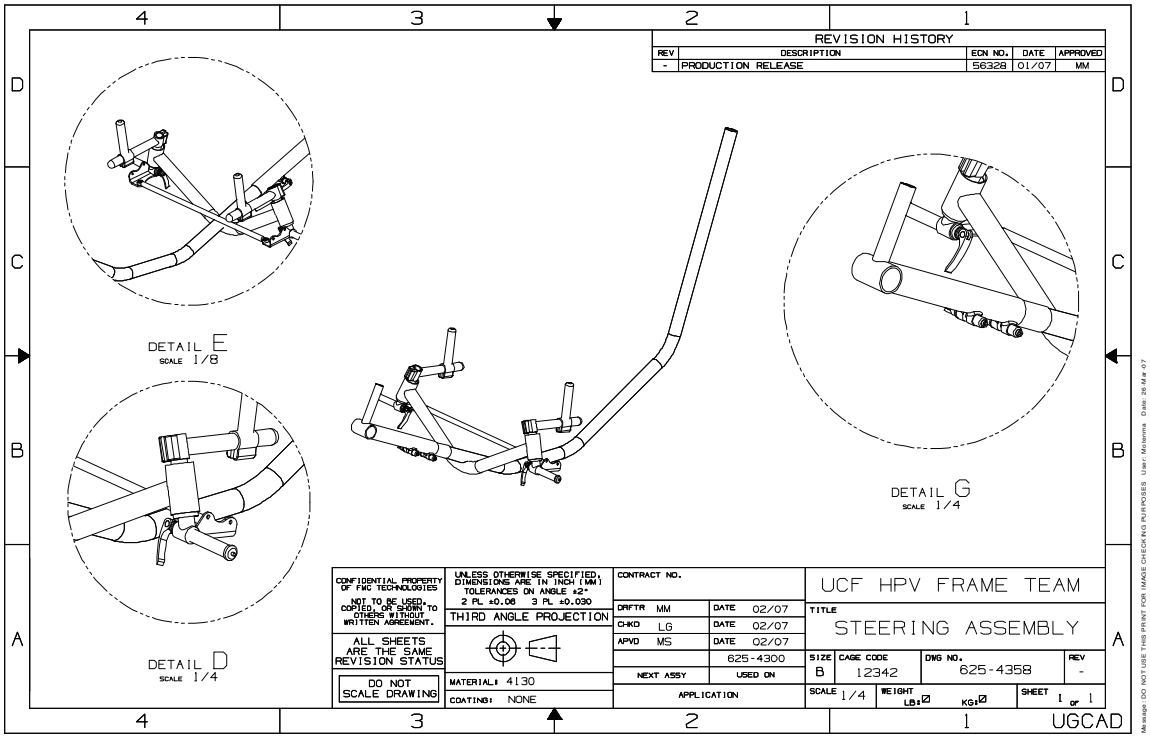

Figure 2.4 Detailed Drawing of Steering and Boom Arm Assembly.

To resist wear, scratching and slipping, a polyethylene material is used as a gasket that fits between the frame and inner wall of the boom. This material will provide a low friction coefficient that will allow the boom to move easily. The bottom of the boom, where it slides onto the frame, is cut and round aluminum tubes are attached on each side of the slot. These tubes are used in conjunction with butterfly clips to provide sufficient clamping power for the boom to stay connected to the main frame. One clip supplies an estimated 100lbf, the amount required to keep the boom attached to the frame. To ensure a factor of safety of 2, two clips are used in the design. The end of the boom contains the bottom bracket housing that was threaded using CNC technologies (24 tpsi in a 32mm diameter housing) that meet the vendor specification required for the external bottom bracket.

UCF's HPV features a fully triangulated rear stay configuration as seen in Figure 2.5. This particular configuration gives the vehicle an excellent support structure for the chain and dropouts as well as distributes the stresses throughout the frame evenly. The rear stays were constructed from normalized 4130 Chrome-Moly steel tubing while the rear dropouts were CNC cut from 0.125 inch mild steel plating. This material selection gives the design strength and stability while providing good weld-ability between components. The configuration of the rear stays depends directly on the selection of the gearing system and the routing possibilities of the chain. For example, the rear dropouts have explicit vendor specification that requires the angle between the Nexus hub's mounting bracket and the lower rear stay to be precisely 38^0, see Detailed View D in Figure 2.5. Moreover, the routing of the chain dictated the configuration of the lower stay relative to the frame's backbone. This was considered early in the design process to avoid chain clashing and design changes during manufacturing such as the addition of another idler wheel.

ASME's roll bar safety requirement was met by designing the main frame of the vehicle to function as the roll bar, see item number 6 in Figure 2.5. The main frame is made from 1.5 by 0.049 inch diameter 4130 (Chrome-Moly) normalized steel. The top of the roll bar was cut to a height that cleared the top of the largest rider's head for the safest roll bar configuration. For additional roll over safety, side supporting roll bars were added to the design to protect the rider from all possible angles. These side supports are made from 0.75 inch by 0.058 normalized steel. The configuration of this safety system is based on head and shoulder dimensions taken during the human fitting process, see Figure 2.5 for configuration.

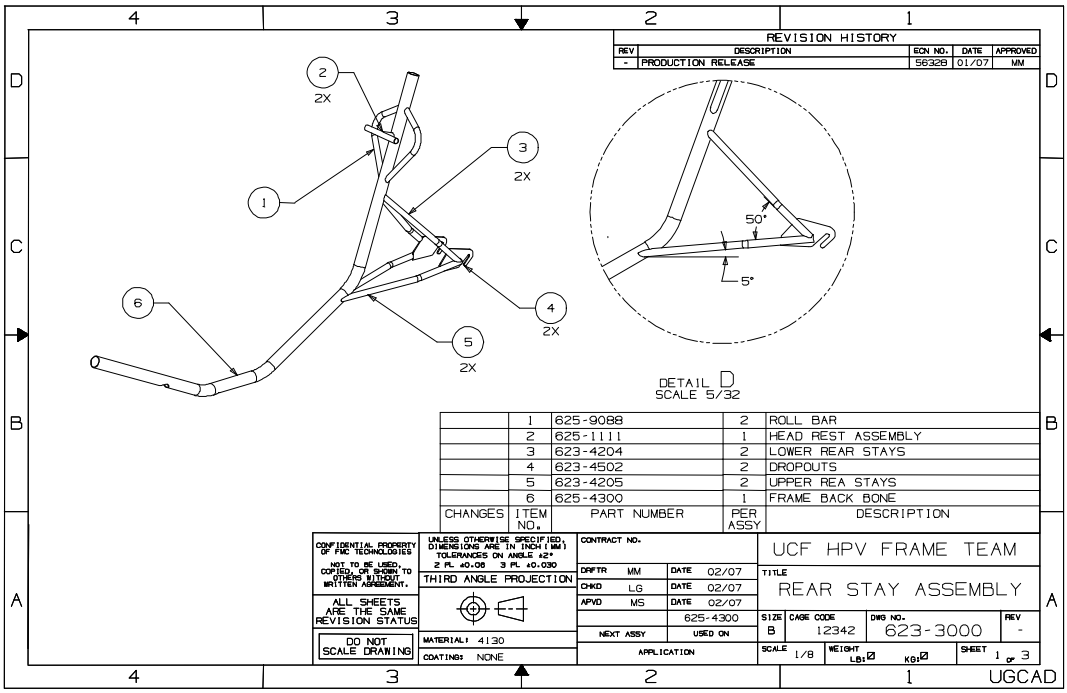

Figure 2.5 Detailed Drawing of Rear End and Roll Bar Assembly.

A custom 2lb ergonomic carbon fiber seat was selected to support the rider's weight while riding. This seat meets all of the human fitting constrains, a back and neck angle of 30^0 and 70^0 respectively, as well as surpasses any of UCF's capabilities of an in house seat construction. Initially a fiber glass composite seat was proposed in the design. This seat was planned to be manufactured using vacuum bagging technologies and high strength fiberglass structural supports. However, the cost of the molds, materials, and time of construction were out of the scope of this particular project's deadline. Nevertheless, this alternative is a step up in manufacturing and material selection.

To attach the seat to the frame, custom seat brackets were designed and fabricated. The seat brackets were designed to be strong, light weight, and work well with the carbon fiber seat selection. Initially, the seat brackets had a one piece configuration that bolted directly to the frame through 0.25 inch holes. However, the Finite Element Analysis of these components produced high stress concentrations in the frames backbone at the connection points due to the holes. This led to a two piece assembly configuration that does not require any holes in the frame's support structures. This particular configuration also gave the design the ability to be flexible in the material selection process. The top seat bracket is constructed from a 5000 series aluminum alloy (5052 H32). This material was selected over 6061-T6 (tempered aluminum alloy) due to its ability to retain its strength after welding in localized locations. It was found through material research that the strength of a 6000 series tempered alloy could drop up to 45% after welding in localized locations and required heat treatments after manufacturing,(**Callister, Jr. 4**). On the other hand, 5000 series un-tempered alloys only loose about 10% to 20% of its strength after welding. This material selection gives flexibility in the manufacturing process by making the part's construction cheap and easy. Heat treatments for material can be very expensive from a manufacturing standpoint and time consuming.

The top seat brackets are designed with a large mounting plate that aids in the distribution of the rider's forces evenly over a large area (i.e. reduces the pressure on that surface). A cylindrical cross member was added to the design to give the bracket more support in the lateral direction when mounted, see Figure 2.6 for reference. A rubber gasket sits between the carbon fiber seat's lower surface and the upper plate of the seat bracket. This will allow the seat to be fastened securely to the brackets without damaging the structural integrity of the carbon fiber seat. Large washers were also used to distribute the loads of the connection bolts to the seat's top surface evenly by reducing the applied pressure. Furthermore,

these plates are custom bent to the curvature of the seat's undercarriage to provide the best possible fit for this component, see Figure 2.6 Detail E for upper seat bracket configuration.

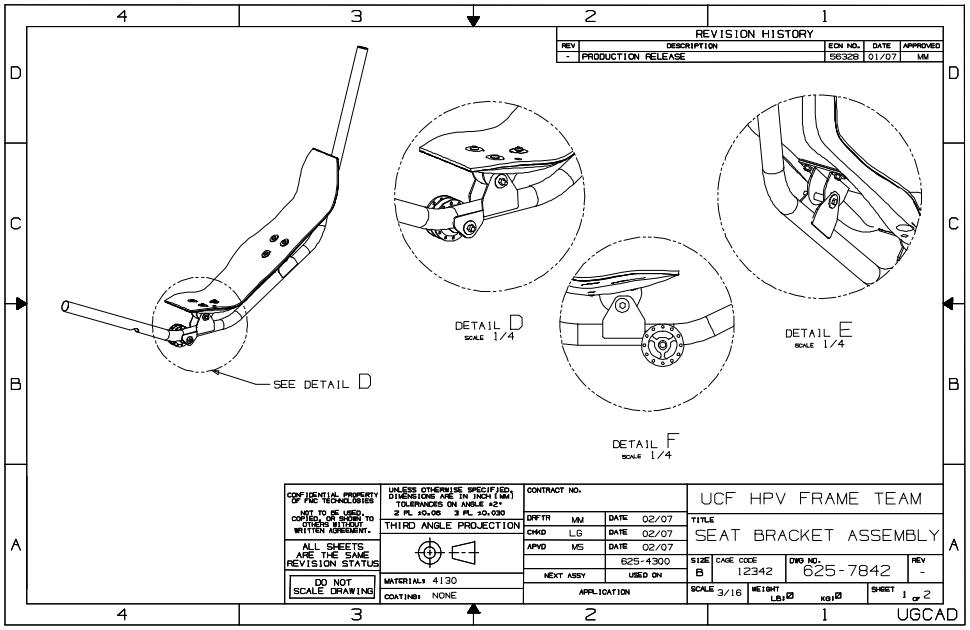

Figure 2.6 Detailed Seat and Idler Bracket Assembly Drawing.

The lower mounting brackets are made from 0.125 mild steel plating that were precision cut using computer guided plasma cutting technology. The design of this bracket serves two functions. First, the bracket's main function is supporting the seat assembly that caries the rider while distributing the rider's forces evenly to the frame. Secondly, the brackets serve as gussets to hinder the vertical deflection of the frame during riding. These gussets will prevent the vehicles idler wheel from coming in contact with the ground due to its low orientation relative to the ground. The idler wheel assembly bracket also serves as a gusset for the frame's backbone, see Figure 2.6 Detail D for reference. This single idler wheel was designed to replace many smaller idler wheels that were incorporated in last year's design. This design will reduce the amount of mechanical frictional losses by reducing the number of contact points with the drive chain. Furthermore, ABEC-7 series bearings were added to the idler wheel assembly to provide a decrease in the rolling resistance. Added strength of this component was achieved by the titanium material selection of this part.

Finally, the fairing supports on this vehicle are designed with five quick release quarter turn Dzus fasteners. This component allows the faring to be easily detached from the frame incase a quick repair is needed to be done to the vehicle or fairing during the competition. This component is most commonly used in the automotive industries as quick release body fasteners. The fairing is attached to the frame by a network of steel arms that are shaped to avoid human contact when entering and exiting the vehicle. The fairing support arms not only function as a supporting structure for the fairing, but they also could protect the rider during a roll over scenario. The supports are made from 0.375 inch normalized 4130 steel tubing for added strength during impact. The triangular configuration gives added strength in the lateral direction and helps absorb heavy impacts, see Figure 2.7 for reference. This added safety parameter would completely protect the rider is any roll over scenario that could be encountered during this competition.

After the modeling of the frame was completed, the overall weight of the frame was computed. Last years frame was a design with two wheels and weighed 15.5lbs. This is not including the weight of any components that were added after the manufacturing process (components that are included in the calculations are the seat, roll bar, rear-end, main frame, and front forks). It is desired to design a frame that is equivalent in weight to last years design with the added safety factor of the extra wheel. This year's frame weight was computed to be 16.5lbs not including the 2lb carbon fiber seat. However, the added weight of the extra components will result in a high over all weight of the frames assembly. The center of gravity of the vehicle was also designed to be as low as possible. This is a very important design feature for three wheeled vehicles to ensure that a roll over scenario is minimized during a high velocity turning

scenario. Last years frame's center of gravity was noted to be 19.25 inches from the ground; however, this year's design features a center of gravity that is 11.75 inches from the ground, see Figure 2.7 for reference.

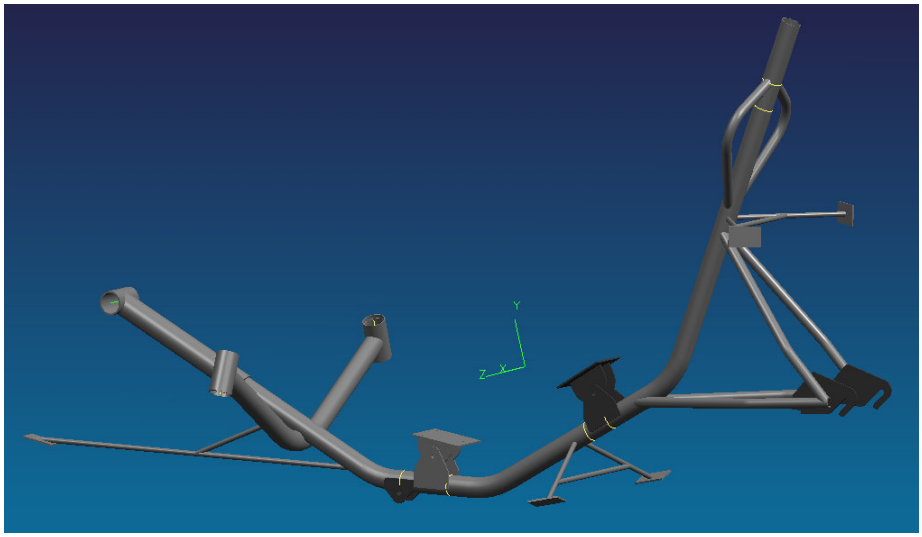

Figure 2.7 Location of the Center of Gravity of the Frame.

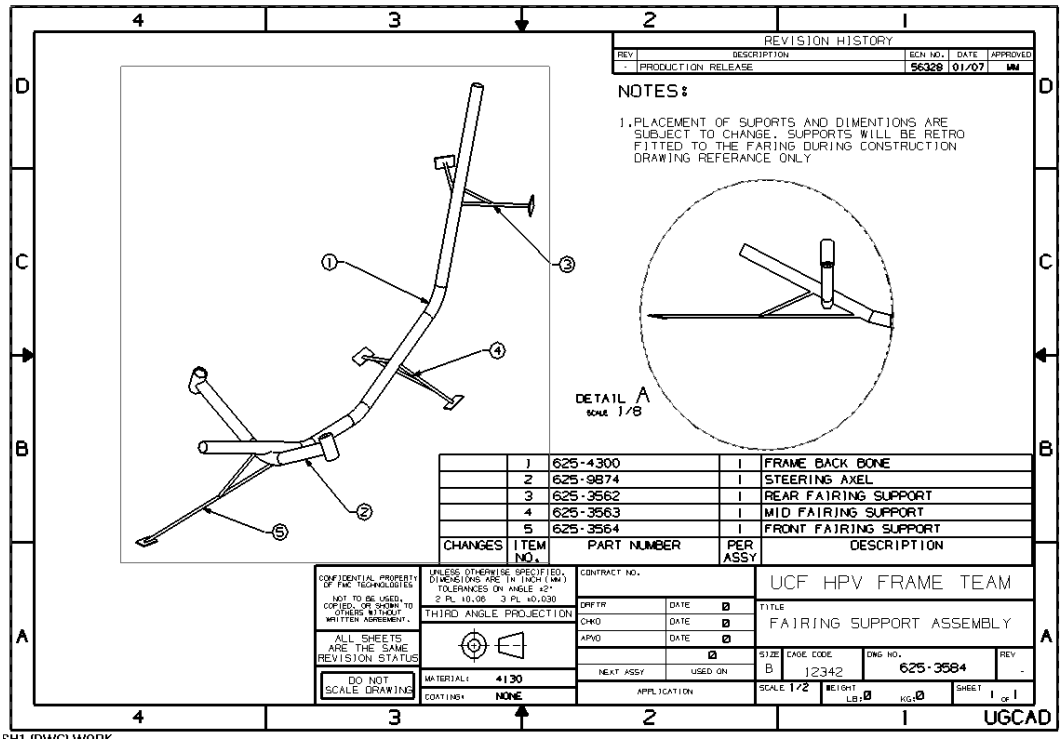

Figure 2.8 Detailed Drawing of Fairing Supports Assembly.

Fairing Design

The aerodynamics of a vehicle dictate the efficiency of the vehicle's power system as well as limit its maximum speed capabilities. Research studies show, done by Dr Joseph Katz from the University of Cambridge, that auto mobiles traveling at speeds over 40mph experience the greatest energy loses due to

aerodynamic drag on the body of the vehicle, approximately 60% and 15% for rolling resistance (Katz, 6). From the initial design criteria, a low riding, streamlined, fully enclosed fairing was selected as the best configuration to limit drag forces on the vehicle. Figure 2.9 shows possible fairing shapes that were considered during the initial design process and their corresponding drag coefficients. From this table it can be seen that a stream lined body will generate the minimum desired drag coefficient. However, this shape is ideal and other contributing drag reduction techniques were considered to produce the best aerodynamic shape possible.

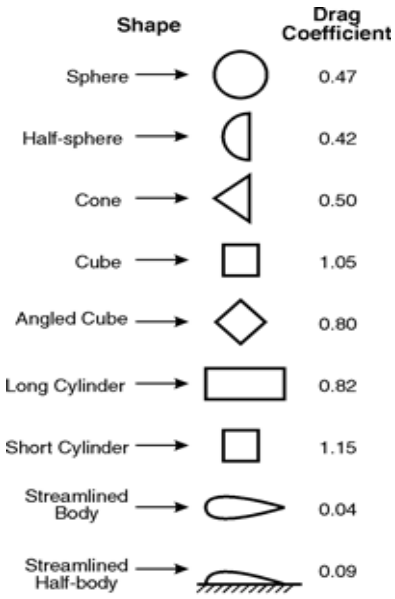

Figure 2.9 Shape/Drag Chart

First, the minimization of the fairing's dimensions will provide the best shape for maximum drag reduction. The length of the vehicle's body will dictate how long laminar flow will stick to the fairing's outer shell. The object is the keep the fluid flow around the fairing in the laminar region for as long as possible. Turbulent flow creates back pressures as well as increases drag forces on any body **(Fox, 7).** The width and height of the fairing must also be kept to a minimum to limit the exposed frontal area that creates high drag forces. For this reason, the fairing as well as the frame, were designed to work in harmony to achieve these goals.

The fairing's overall width was limited by the frame's wheel track dimension (33 inches). The fairing's outer walls were designed to sit flush with the two front wheels. Fiberglass wheel disks were fabricated to cover the spokes of each wheel to eliminate the "egg beater" effect they cause while at rotation at a high angular velocity. The height of the fairing (39 inches) was dictated by the largest rider's body dimensions that were taken during the human fitting process. To create the minimum cross sectional area of the fairing, a computer generated human model was imported into the frame's assembly, see Figure 2.10 for reference. The human model was within 95% of UCF's largest riders body dimensions which will dictate an accurate model of the fairing relative to the actual riders.

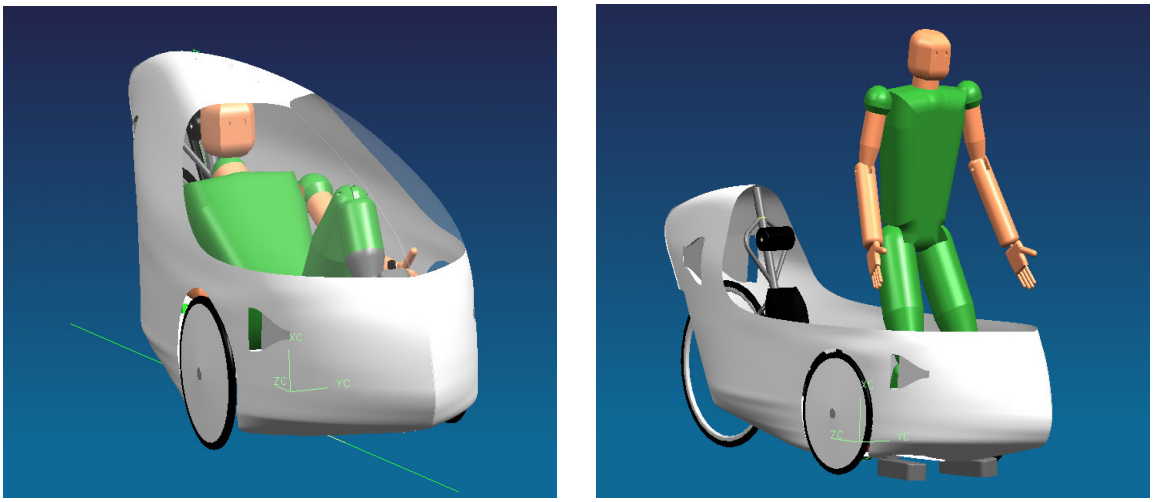
Figure 2.10 Human Modeling of Mock Rider

The desired ground clearance of the vehicle was set to be less than 5 inches based on preliminary research. Both positive and negative lift can be generated as a result of a body being placed too low to the ground. Some positive lift is useful in an HPV design to limit the blunt weight of the fairing, but the trade-off of positive lift is a larger drag coefficient and consequently more drag. Figure 2.11b shows the drag and lift coefficients v.s the ground clearance height to overall length ratio of a vehicle designed with a 10^0 tapered lower surface. A longer vehicle will have a lower lift coefficient, but the vehicle may experience premature Laminar flow separation. The final fairing length was set to be 92inches with a minimum fairing ground clearance of 3.5inches. Calculating the height to length ratio (h/L=0.038) it can be readily seen that

the lift can be minimized while sustaining a high drag coefficient. This calculation is based on a tapered rear end angle of 10^0 from the horizontal which is incorporated in the fairing's final design.

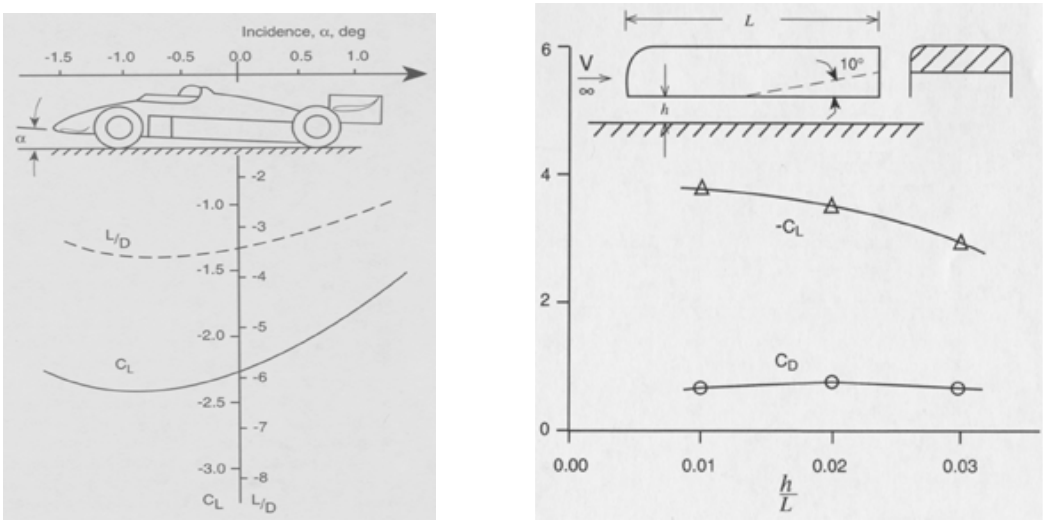

Figure 2.11a, b Lift and Drag Coefficient Charts at Reynolds Number equal to $3x10^6$.

Next the angle of attack of the front lower portion of the fairing was designed based on Figure 2.11a. This specific angle will dictate the lift capabilities of the faring as well as the drag forces associated with it. The angle of attack is a direct function of the lift; therefore, an 8^0 inclination was used in the first 24 inches of the lower surface from the leading edge of the fairing, see Figure 2.12 for reference. This design parameter should provide minimal lift capabilities while minimizing the drag losses.

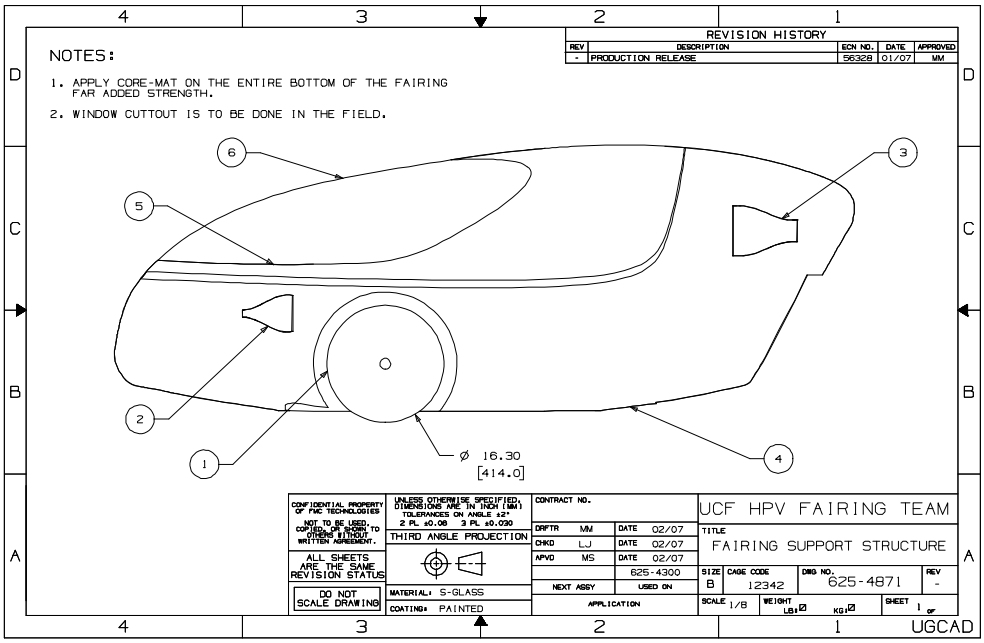

Figure 2.12 Final Fairing Design Shape.

During the endurance race minimizing the rider exchange time is curtail for a fast over time. The three wheel designed frame will add stability to the vehicle during the exchange without the aid of a team member holding the vehicle upright. However, the rider must have some kind of stable platform to stand on while exiting. The solution to this problem is two small foot cutouts that will allow the rider to stand up and exit the vehicle quickly. The locations of these cutouts are located directly behind the leading edge inclination. The reason for this strategic location is to minimize the air flow coming into the vehicle from beneath. Furthermore, the cutout dimensions are minimized to just allow enough room for the rider's feet to

pass through without damaging the fairing in the process. This design feature should allow for a rider exchange time to be less than 25 seconds.

Rider Cooling Concepts

Rider ventilation and cooling is also a huge design parameter for any HPV design. The average mid-day temperature in the Orlando metropolitan area (the site of the 2006-2007 East Coast HPVC) can reach as high as 87^0F on average during the month of May. This extreme temperature is not the only weather concern for outdoor activities. The average humidity percentage during the same time period can reach 89% (**Johson, 4).** Furthermore, it was found that the average cyclist could sustain a power output of 0.5Hp (373 Watts) for about 5 to 15 minutes (Wichers Schreue**, 5**). A world class HPV athlete would have to sustain the same power outputs to achieve a world record time. With an average of 25% for thermal efficiency of a human being in excellent condition, the excess heat a rider produces can be calculated by the following equation.

Equation 2.2 Equation of Heat Produced by a Rider $$Q = \left[\frac{1-f}{f}\right] \cdot P$$

Where Q is the excess heat and *f* is the thermal efficiency, and P is the power of the rider. Using this equation, the excess heat a rider produces is 1119 Watts. This heat will need to be cooled for the person to ride comfortably inside the fairing. Due to these conditions, it is extremely important to design a vehicle that incorporates a human cooling ventilation system

There are two ways to cool a rider during athletic activities in a HPV. First, a convection cooling process can be achieved by allowing air to flow over the rider's body. The rider's face as well as the midsection is the most important cooling locations for this process. Secondly, an evapotranspiration process which allows the human body to produce sweat naturally, cools the rider during a race. However, the rider fluid loses must be replenished to maximize this cooling process. According to the study by Abbot and Wilson, the average fluid losses a rider can experience is a little over 1 liter per hour. The average cruising speed in the endurance race is desired to be 20 – 25 mph for an approximate duration 7- 8 miles per person. Therefore, the average ride time per person for this event is 25 minutes, so each rider could perspire up to 1 liter of fluids during this period of time.

The solution for the convection cooling process is a NACA duct air ventilation system. NACA ducts are designed to give a maximum air flow rate while minimizing the drag losses to the aerodynamics of the vehicle. The ducts are placed in a location that will allow the air to flow over the riders chest and face during the race. The front inlet ducts are designed with a smaller duct area then the rear ducts. This is to ensure that the mass flow rate of cool air through the vehicle will always positive. The optimal diverging submerged NACA duct is designed with a duct angle between 5^0 and 7^0 and a width to depth ratio between 3 and 5 (Mossmen**, 5).** Based on these findings, the front inlet duct will employ a 7^0 ramp angle with a 3:1 width to depth ratio. The width of the inlet duct was set to 5 inches, 1.6 inch duct depth, which results in a 0.11 lb/s mass flow rate of air at 20 mph and 0.22 lb/s at 40 mph. The rear duct will employ the same duct angle of 7^0, but with a higher width to depth ratio of 5:1. From this, the exit duct was designed with 7 inches duct width, a 2 inch duct depth, which results in 0.19 lb /s mass flow rate of air at 20 mph and 0.38 lb /s at 40 mph.

Fairing Material Selection

The material selection for the fairing must be strong enough to withstand any pressures that are derived from wind resistance during a high velocity scenario. It must also be safe and durable enough to withstand small impacts and have material characteristics that are safe if fracture occurs. Composites such as fiberglass, carbon fiber, and Kevlar were initially considered because of their material properties. Carbon fiber is the best material selection for this particular application due to its high strength to weight ratio. Unfortunately, it is the most expensive and scarce composite that was considered. The next best possible material that is available is a fiberglass composite structure. Fiberglass is relatively light weight, easy to manufacture, and strength can be added to the material by stiffening agents such as Core-mat and K-mat.

Two types of glass were considered as a possible material that would make up the fairing's outer shell. The first fiberglass is E-glass (electrical glass). E-glass is light weight and is one of the cheapest cloths in the fiberglass family. The second glass is S-glass (strength glass). S-glass is slightly heaver than

E-glass, but its strength is far greater. Structural rigidity can be added to the fairing by the use of a K-mat or Core-mat fabric. K-mat is laid up between layers of glass to add rigidity and increase hardness on the surface. Core-mat is also laid up between glass surfaces; however, it requires much more resin to saturate the glass and the mating and is also a very heavy alternative. However, Core-mat is much easier to manufacture than K-mat in a complicated structure like this year's fairing design.

Fiberglass Material Testing

Initial research was conducted to arrive at a conclusion for the best material configuration selection for the structure of the fairing. Non-isentropic material (composites) properties depend directly on the manufacturing process while their strength depends on the resin concentrations in the cloth as well as the ounce of cloth used. Material testing will provide a good weighing scale for the best possible material selection. Several different types of material configurations were tested.

Initial Material Configuration for Testing.

A. Two layers of 9oz E-glass with epoxy, K-mat and micro-bubbles, then another two layers of 9oz E-glass with epoxy.
B. Two layers of 9oz S-glass with epoxy, K-mat and micro-bubbles, then another two layers of 9oz S-glass with epoxy.
C. Two layers of 9oz E-glass with epoxy, Core-mat, then another two layers of 9oz E-glass with epoxy.
D. Two layers of 9oz S-glass with epoxy, Core-mat, then another two layers of 9oz E-glass with epoxy.
E. Four layers of 9oz E-glass and epoxy.
F. Four layers of 9oz S-glass and epoxy.

The best material will provide a light weight and strong solution. The first elimination was done by performing an impact test on each sample. Ten uniform samples of each material configuration were cut and placed in an Izod impact testing machine, see Figure 2.13b for reference. The purpose of this experiment was to study the fracture characteristics of S-glass and E-glass in the case of an impact that would cause a failure in the fairing's structure. The conclusion of this test showed that E-glass, in each configuration, would completely fracture upon impact and leave sharpe particle on the fracture surface. This was ruled to be a very unsafe material selection, so E-glass was eliminated from possible solutions.

Figure 2.13a Tensile Testing Machine

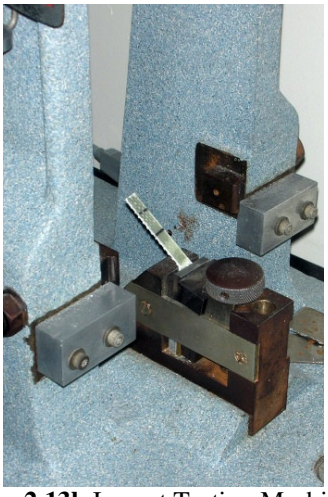

Figure 2.13b Impact Testing Machine

Next, a tensile testing experiment was conducted to separate the difference in strength between each S-glass sample. It is desired to find the strongest material with the lightest weight configuration. Ten samples of each configuration were pulled to fracture and the strength of each was averaged and recorded. Figure 2.14 shows the stress strain plots of the three samples that were tested (sample B, D, F form the configuration diagram). From this data the K-mat sample is the strongest material configuration; however,

it is also the most dense sample which will result in a heavy material. Core-mat is shown to have a lower ultimate tensile strength with an equivalent modulus of elasticity. It is also twice as strong as a sample without a support structure. This material is also easier to manufacture and was chosen for further testing.

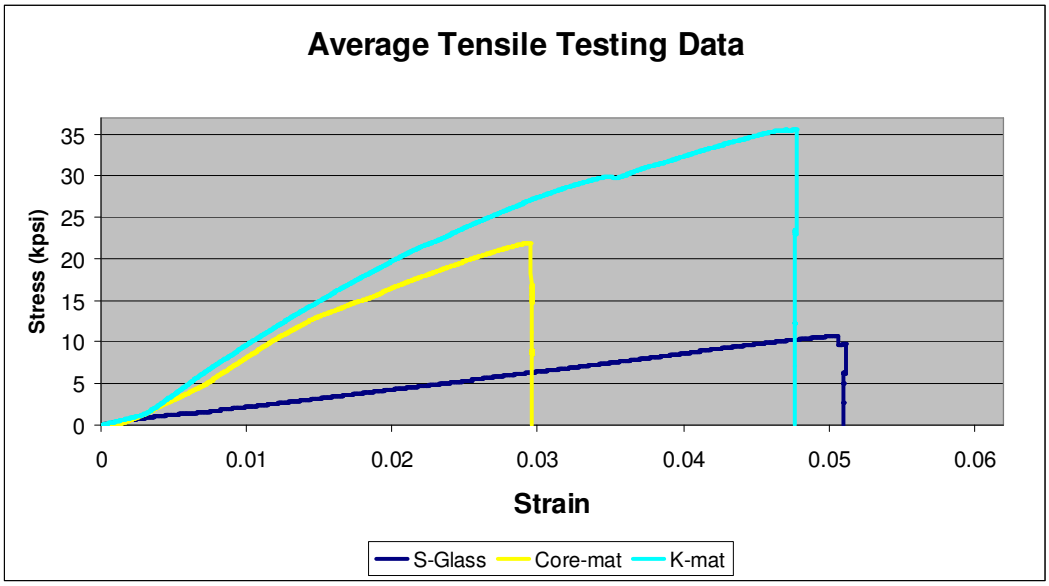

Figure 2.14 Stress Strain Relationship for Core-mat, K-mat, and Regular Glass Samples

Next, the number of layers that will be needed in the construction of the fairing was selected by the use of another tensile testing experiment. This experiment will show the difference in strength by the addition of layers of fiberglass in the Core-mat structure. Two, three, and four layered samples were laid up in a Core-mat sandwich and tested. Ten samples of each layering configuration were tested up to their breaking points. Figure 2.15 shows the stress strain results of this experiment. This data shows that the difference in strength as each layer is added grows more rapidly depending on the amount of layers that are applied to the test sample. For this reason, 4 layers of S-glass with a Core-mat strengthening structure was selected as the best material for the fairing construction.

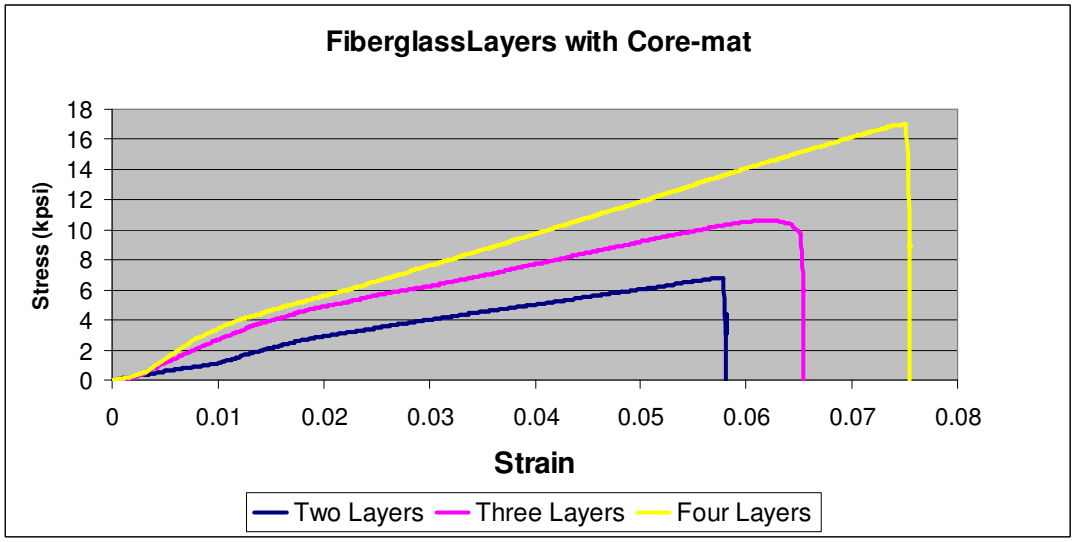

Figure 2.15 Stress Strain plot for Different Glass Layering

The amount of Core-mat that will be used depends on the cutouts in the fairing. Last year's design used a completely enclosed strengthening K-mat membrane that made the fairing very heavy and very strong. For this reason, a Core-mat skeleton concept will be implemented in the fairing design. This design

feature will add strength to the weak spots in the fairing and keep the weight down in areas that do not need support. Initially a FEA was attempted on the fairing and the strengthening Core-mat skeleton; however, non-isentropic materials in a complex FEA solver take a long time to solve. Unfortunately, UCF does not possess computers fast enough for such a task and this method was abandoned. Figure 2.16 shows the areas that were strengthened by the use of Core-mat. The major areas of concern for strengthening are the those that are being cutout due to rider mobility. The entire bottom of the fairing was to be covered with Core-mat for added strength to limit the movement of the body when riding. The canopy flange will also be supported by extra material for added support. Each fairing mounting point will be strengthened due to the quick release D-zus fastener that will be riveted to the faring.

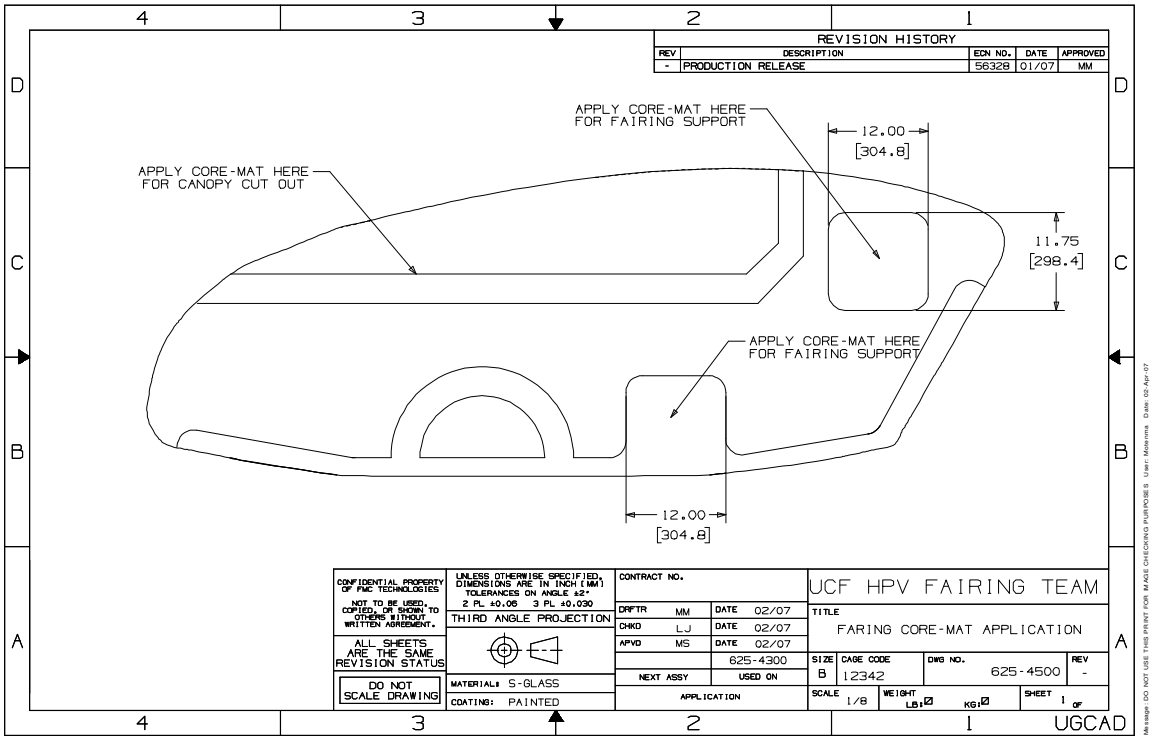

Figure 2.16 Core-mat Skeleton Strengthen Structure

Analysis

Finite Element Analysis

All the Finite Element Analysis (FEA) for this year's vehicle was done using UGS Nx3 engineering based software. Nx3 comes fully equipped with an assortment of CAD/CAM/CAE applications, such as human modeling, assembly design, kinematics simulation, and a Nastran based finite element solver. All the FEA scenarios were estimated from the worst possible situation the frame could withstand during ASME's HPV event.

Breaking Scenario

The first simulated scenario was an extreme braking situation that could expose the frame's steering axle to severe bending and axial loads. To calculate the braking forces needed to meet ASME's minimum braking requirements, stopping with in 20ft at 15mph, the work energy principle was used with the team's heaviest rider in mind (220lbf),. This calculation led to a braking force of 51lbf for each wheel. This scenario is a minimum requirement and much larger braking forces could be encountered in the sprint or endurance events. For example, if UCF's HPV was surrounded by other competing vehicles during the endurance race and the lead vehicle crashed or experienced a roll over, UCF's rider would have to respond and stop within a distance of approximately 25ft at a rate of 20mph to avoid an accident. This would result in the worst

possible braking scenario force of 71lbf per wheel. Figure 3.1 shows the stress diagram plot of all the frame components that are affected by these applied loads.

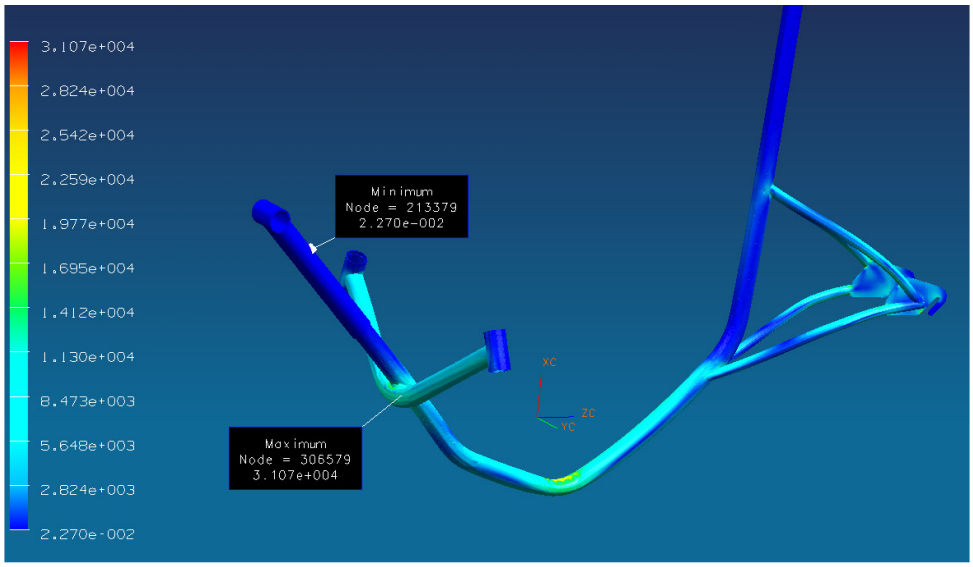

Figure 3.1 Stress Diagram During Worst Case Braking Scenario.

This scenario was bounded by fixing the rear dropouts in all direction and allowing the two front head tubes to move in the horizontal direction but not the vertical. The applied loads due to the rider's weight (220lbf) were applied at the location of the center of gravity of the vehicle and distributed to the frames backbone at the approximate locations of the seat brackets. The braking forces were applied using bearing loads on the inside portion of each head tube. The maximum Von-Misses stress was found to be 31kpsi located near the joint of the frame and the steering axle. This analysis provides a safety factor of 2:1 and a maximum deflection of 0.14 inches.

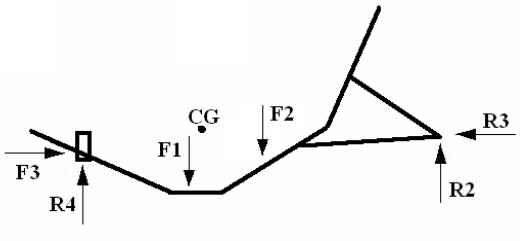

$$\sum F_x = 2F_3 - 2R_3 = 0$$

Where $R_3 = 71lbf \leftarrow$

$$\sum F_y = 2R_1 - F_1 - F_2 + 2R_2 = 0$$

$$\sum M_{R_1} = 11.81F_1 + 29.19F_2 - (48.13)2R_2$$

Where $R_2 = 45lbf \uparrow$ and $R_1 = 65lbf \uparrow$

Figure 3.2 Free Body Diagram During Braking Scenario.

To verify that the computer analysis is correct, the reaction forces were found analytically and compared to the simulation's reaction forces; see **Figure 3.2** for calculations. Table 3.1 shows the brake down of the hand calculation results and the corresponding percent error. The ultimate goal is to have all of our modeling solutions accurate within 8% of our analytical solution. From this data, the maximum difference in the model solution is 5.3%, which is satisfactory for this team.

Reaction	Model FEA (lbf)	Hand calc (lbf)	Difference (lbf)	% Difference
Head tube Left	68.6	65.1	3.5	5.3
Head tube Right	68.9	65.1	3.8	5.8
Dropout Left	47.6	45.2	2.4	5.3
Dropout Right	47.6	45.2	2.4	5.3

Table 3.1 Hand Calculation Verification Data

Pedaling Scenario

The second scenario was derived to verify that the frame's design was capable of withstanding the worst possible pedaling forces. This scenario tests the frame's reaction to a high pedaling force from a stationary position while in a low gear. For this analysis, the deflection in the frame is a very important parameter to minimize so the rider's energy can transfer to the rear wheel efficiently. Large deflections in the frame's components are due to the rider's applied forces; however, these human forces are intended to power the vehicle instead of deforming the vehicle's structure. The applied pedaling force was simulated as a bearing load applied to the inner wall of the bottom bracket housing with a magnitude of 200lbf. The largest rider was also assumed in this simulation to provide the worst possible loading scenario. The reaction forces of the rider's back to the seat during pedaling, was calculated using a free-body-diagram. These forces were applied, as bearing loads, at the exact location of each seat bracket. Figure 3.3 shows the stress diagram of all the frame components that are affected during this scenario.

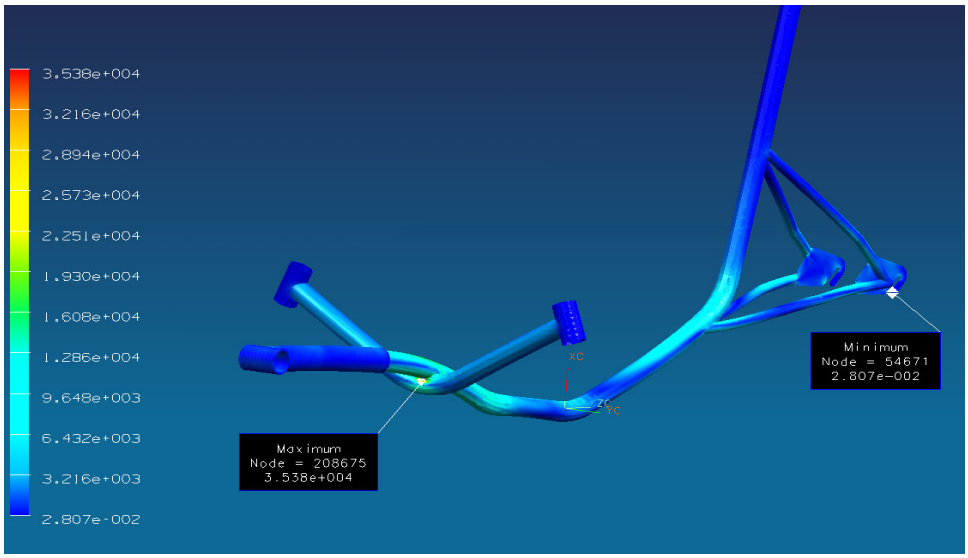

Figure 3.3 Stress Diagram During Worst Case Pedaling Scenario

This scenario was bounded to fix the rear end dropouts in all directions and simply support the two front head tubes. It is also important to note, this scenario has two dissimilar materials that are being modeled at the same time. The boom arm is made from 6061-T6 aluminum while the frame's backbone is Chrome-Moly steel. These materials cannot be welded conventionally and must be meshed separately in the model. To join this assembly a mash mate command was used to create coincident nodes between the frames backbone and the inner wall of the boom arm. Small tetrahedral meshes were created to join the two structures together so they can be constrained to move in unison. The maximum von-Mises stress was found to be 35.3kpsi located at the point were the frame meets the steering axle. This simulation results in a safety factor of 2:1 and a maximum deflection of 0.16 inches. These results act within the elastic limits and engineering stress-strain relationship as well as provide a maximum deflection that is less than a quarter of an inch.

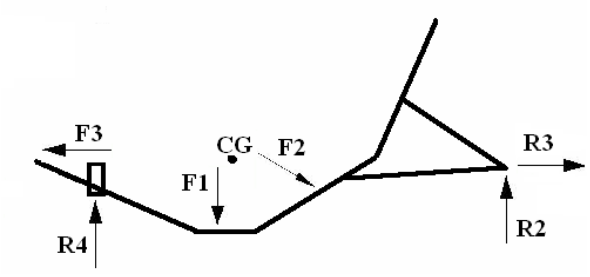

$$F_P = 200lbf \leftarrow \quad W_R = 220lbf \downarrow$$
$$\sum F_y = F_2\cos(60) + F_1 - W_R = 0$$
$$\sum F_x = F_{1x} + F_P - F_2\sin(60) = 0$$
$$\text{y-comp } F_1 = 126lbf \downarrow$$
$$\text{x-comp } F_1 = 165.9lbf \rightarrow$$
$$F_2 = 108lbf \ @ \ -60^0$$

Figure 3.4 Free Body Diagram During Pedaling Scenario.

To verify that the simulation is producing accurate results based on the applied forces; the model solution was compared to analytical calculations and free-body-diagrams. Table 3.2 shows the breakdown of all the reaction forces as well as the percent difference in the calculation. The maximum difference in this solution was found to be 6.9% which is within our standards for this particular scenario.

Reaction	Model FEA (lbf)	Hand calc (lbf)	Difference (lbf)	% Difference
Head tube Left	72.5	68.8	3.7	5.3
Head tube Right	72.6	68.8	3.8	5.3
Dropout Left	43.8	40.9	2.8	6.9
Dropout Right	43.8	40.9	2.8	6.9
Rear X-Comp	198.9	200	1.1	0.5

Table 3.2 Pedaling Hand Calculation Verification and Error

Seat Bracket and Idler Wheel Loading

The third Finite Element Analysis was preferment on the seat brackets as well as the idler bracket assembly. The purpose of separating this scenario's components from the other two is for several reasons. First, the overall structure of the frame can be meshed more accurately if the model file contains a simpler structure. This will allow the computer software to produce attractive tetrahedral meshes with an average aspect ratio for the model close to a unit ratio. Secondly, memory space and solution solving time is a large factor for this strategy. Large files with complicated boundary conditions, mesh mating conditions, and applied forces take a long time to solve. Finally, this scenario will help prove that the design components that are being modeled can withstand the worst possible applied loads as well as produce the desired design function. For example, the lower seat brackets and the idler wheel brackets were designed to add strength to the frame's backbone by acting as gussets.

To analyze these gussets, the frame was subjected to braking scenario forces and the maximum deflection will be noted and compared to the previous solutions. The rider loads will be modeled as pressures and applied to the top seat plate of the seat bracket assembly. The pressure was assumed to act normal to the plate with a magnitude of 11psi for the front bracket and 10psi for the rear. Since the upper seat brackets were designed with two different materials the mesh–mate command was used to constrain the two parts. In reality, a 0.25 inch bolt will hold these two parts together and support the rider's weight. Coincident nodes were formed at the location of the mounting holes in the upper bracket to act like a spider node. The material properties for the aluminum seat brackets were adjusted to correlate with the 20% strength reduction due to welding as discussed before. This will give the worst possible material state that the brackets could be in after manufacturing.

Figure 3.5 shows the stress concentrations in the seat brackets under the worst possible loading scenario. The maximum von-Mises stress was found to be 21kpsi with a maximum deflection in the frame of 0.11 inches. It is important to note that the maximum stress is located in the bend of the frame and not in the seat brackets during this scenario. The maximum von-Mises stress concentration in the upper seat bracket was found by nodal analysis to be 4.7psi . This results in a safety factor of 2:1 and verifies that the material selection in the brackets can with stand the worst possible scenario. Furthermore, the overall deflection of the frame relative to the absolute coordinate system was compared to the previous braking solution. The frame experienced a maximum deflection of 0.2 inches without the gusseting and 0.11inches with the gusseting. The maximum von-Mises stress was also noted to decrease to 21.3kpsi with the gussets in place. This solution raised the over all safety factor of the frame to a 3:1 and verifies the function of the seat and idler wheel bracket design.

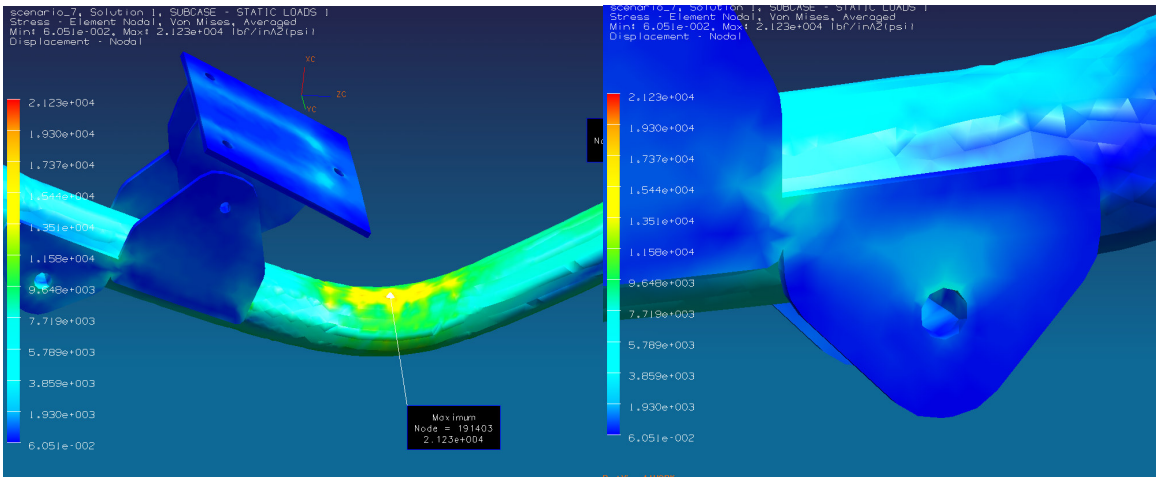

Figure 3.5 Stress Diagram on the Front Seat Bracket

The idler brackets will be subjected to a coupled moment due to the reaction forces of the chain. This scenario is more apparent in the previous pedaling scenario because the maximum pedaling force will be applied to the chain which directly affects the idler wheel brackets. The applied coupled moment was modeled as duel bearing load with a magnitude of 263lbf that result in a moment of 38ft-lbf. These forces were applied to the brackets as a bearing load to simulate the reaction forces of the bolt that transfers the moment. Figure 3.5 shows the stress distribution on the idler wheel brackets based on the applied coupled moment. The maximum von-Mises stress concentration was found to be 17.5kpsi with a negligible deflection in the bracket. This analysis results in a safety factor of 4:1 witch insures that the brackets can withstand the maximum amount of torque that can be applied.

To verify this scenario, the reaction forces were calculated analytically and compared to the modeling solution. Table 3.3 shows the break down of our hand calculations compared to the computers solutions. The maximum percent error in this solution was recorded to be 5.9%. This error is within the desired range of the total error in the modeling solution and our analytical calculations

Reactions	Model FEA (lbf)	Hand Calc (lbf)	Error (lbf)	% error
Head tube Left	72.9	68.8	4.1	5.9
Head tube Right	72.9	68.8	4.1	5.9
Dropout Left	42.1	40.9	1.2	2.9
Dropout Right	42.3	40.9	1.4	3.4

Table 3.3 Modeling and Hand Calculation Breakdown for Brackets

Fairing Supports and Rollover Scenario

The last scenario that was analyzed is a rollover scenario of the vehicle; however, this scenario is very unlikely to happen during this competition's environment. To start, Figure 3.6 shows the location of the center of gravity of the entire frame without any components. This position is important because the low center of gravity of the frame will also ensure that the vehicle will unlikely be in a rollover scenario. From our calculations, the vehicle must maintain a constant velocity of 20mph and turn in a 15 foot radius circle in order to roll over. However, ASME rules only requires that the vehicle can turn in a 25 foot radius circle or greater; therefore, our vehicle will never be exposed to these conditions. Never the less, this scenario is still not impossible and needs accurate analysis to ensure the safety of the rider as well as prove that the safety design features are sound.

For this scenario the fairing support structure, roll bar, and head tube will be the locations of the applied forces due to roll over. To find the direction of the applied forces the frames model was manipulated into a position were the frame would most likely make contact with the ground. The directions of the forces were assumed to be normal to the ground at all the applicable points. To simplify the meshing

process the front fairing support was not modeled because it will never come in contact with the ground during this scenario. The boundary conditions were set up to fix both of the rear dropouts in all directions while fixing only one of the head tubes, located on the opposite side of the impact faces, in all directions.

Figure 3.6 shows the deflection diagram of the fairing supports during the roll over scenario. The maximum deflection of the fairing supports was found to be approximately 0.5 inches located at the rear most fairing support. This is because the head tubes along with the rear most support will have to absorb most of the impact forces due to the orientation of the ground and the vehicle. The maximum stress was found to be 29.5 kpsi located at the point were the rear fairing support is welded to the frame. This resulted in a safety factor of 2:1 witch is satisfactory for this safety analysis.

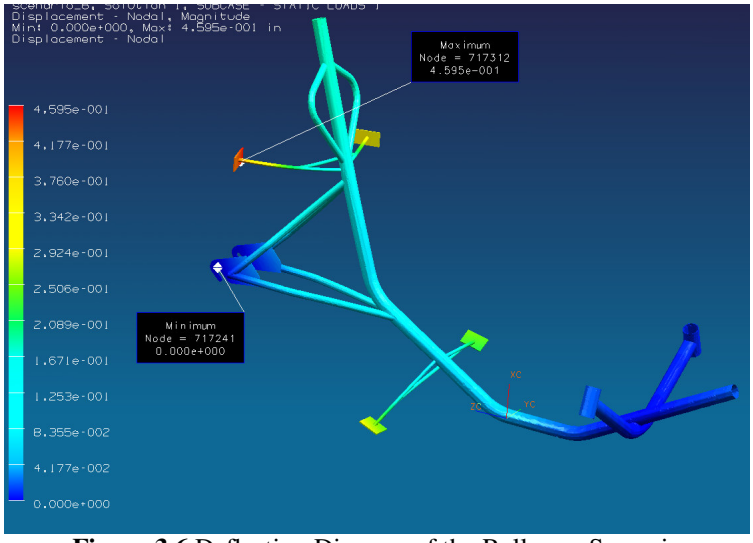

Figure 3.6 Deflection Diagram of the Roll over Scenario

CFD analysis

Computational fluid dynamics (CFD) is the study of fluid mechanics that uses numerical methods and algorithms to solve and analyze scenarios that involve fluid flows. The use of COSMOS FloWorks was employed to develop drag, velocity and pressure gradient information, which was then analyzed to aid in the design of the fairing. CFD is used to develop continuous flow characteristics using a discrete method of analysis. This method allows for a computer to successively develop and simulate the interaction of fluids with complex surfaces. The CFD code runs algorithms to perform multiple calculations of the Navier-Stokes Equation, which can define any single-phase fluid flow.

Equation 3.1: Navier-Stokes Equation $$\frac{\partial}{\partial t}\iiint QdV + \iint FdA = 0$$

This equation presents Q which is the vector of conserved variables, F which is the vector of fluxes set apart in the Navier-Stokes Equation, V the cell volume, and A the cell surface area. This is the fundamental code used in COSMOS FloWorks. This software also returns coefficients of drag (CD), visual plots of the pressure and velocity profiles to better understand the dynamics of the fairing. Validation of the results from this software will later be performed by wind tunnel testing.

The pressure distribution of the fairing was modeled, shown in Figure 3.7, in order to quantify the change of static pressure. For the application of this project, the team assumed a flow velocity of 50 ft/s. This flow velocity represents the estimated race speed during the competition.

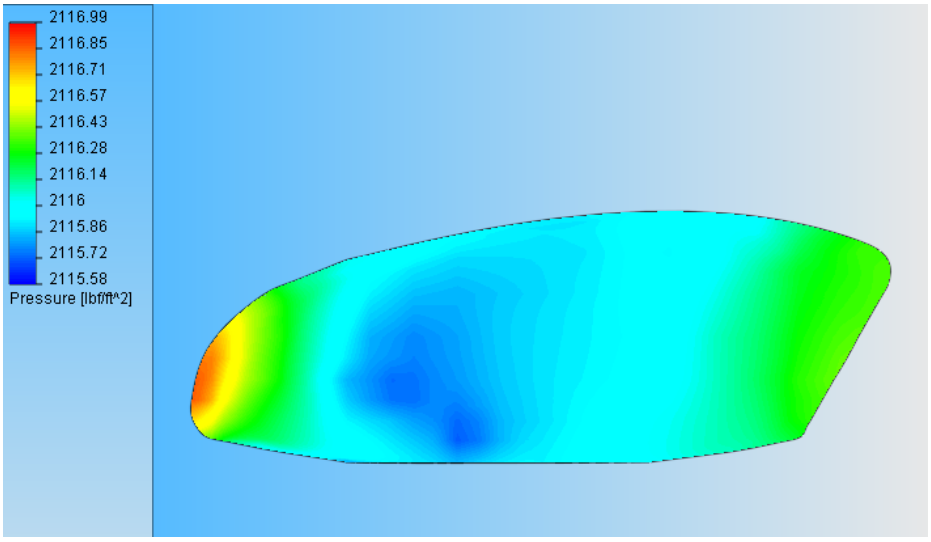

Figure 3.7 Pressure distribution

The fairing has an accumulation of high pressure at the nose, due to stagnation effects. The pressure continues to decrease throughout the fairing.

The placement of NACA ducts on the fairing is dependent on these results. The desired placements of the NACA ducts are areas of high pressure. The ideal placement of the NACA duct would be at the nose of the fairing where the pressure is at a maximum. However, due to increased effects of drag, this location would reduce the performance of the fairing. Therefore, there is a tradeoff between how much air can pass through the NACA duct vs. the disturbance the NACA duct creates. The blue shaded areas are areas of moderate pressure. The NACA ducts need to be placed right on the outer "ring" of this blue area to achieve a balanced performance. This area is about 14.5 inches from the bottom of the fairing and around 18 inches from the nose of the fairing.

The drag coefficient CD, is the dimensionless quantity that describes the amount of aerodynamic drag caused by a fluid flow. The CD is the coefficient expressed in the drag equation shown below.

Equation 3.2: Coefficient of Drag $$F_d = \frac{1}{2}\rho v^2 C_d A$$

In the equation above, F_d is the force due to drag effects, ρ is the density of the working fluid, v is the velocity of the fluid and A is the effective cross-sectional surface area. Using COSMOS FlowWorks the fairing has a CD of .25. This number would seem low but the design of the fairing optimizes air flow therefore resulting in a low CD. The effective frontal cross-sectional surface area was 143.64 in².

The fairing will be subjected to various speeds during the competition. During the sprint, the vehicle will be traveling at the highest velocity possible. During the endurance portion, the vehicle will be experiencing periods of low, moderate, and high speeds. These speeds can range from 32 ft/s up to about 51 ft/s.

It is important to know the velocity distribution that will be experienced on the surface of the fairing in order to quantify how much the air is being slowed down. The velocity profile for the low speed scenario of 32 ft/s is shown in Figure 3.8.

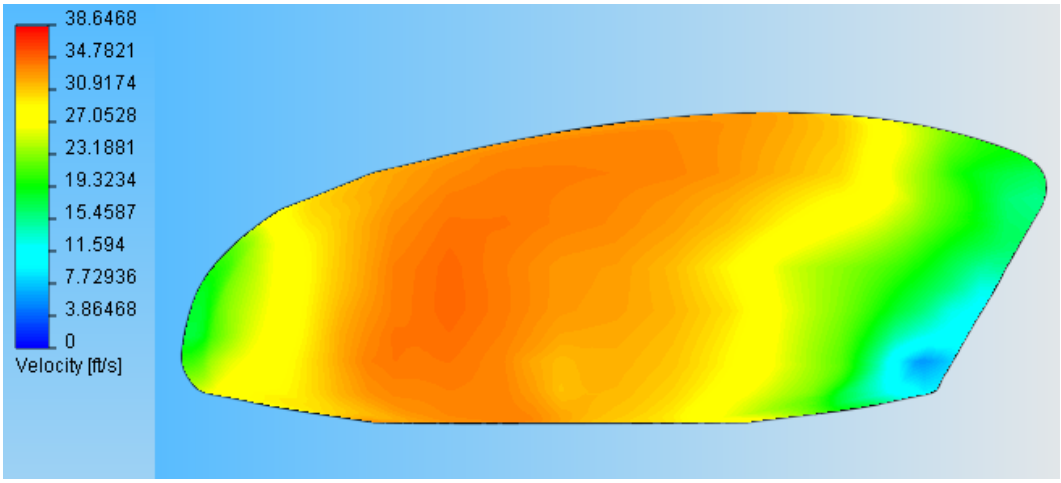

Figure 3.8 Low speed velocity profile

Figure 3.8 clearly shows how the velocity of the air is accelerated through the nose of the fairing to a maximum velocity of approximately 35 ft/s. As air travels across the fairing, the velocity of the air begins to decease shortly after the widest part where the wheels are located. This decrease occurs towards the rear of the fairing to approximately 10 ft/s. This drastic decrease in the velocity of the air is attributed to the effects of flow separation due to an unfavorable pressure gradient. The velocity profile for the high speed case (51 ft/s) is shown in Figure 3.9, below.

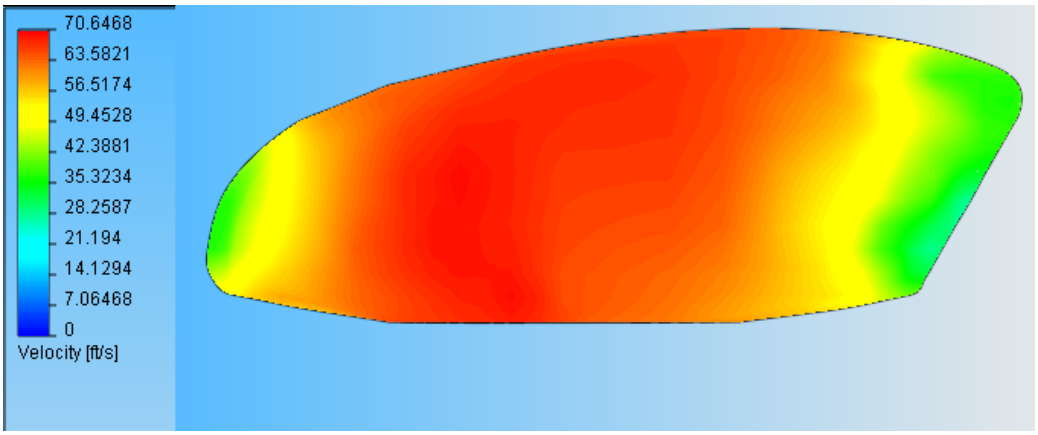

Figure 1.9 High speed velocity profile

The high speed velocity profile returned similar results as the low profile. The air is accelerated through the widest part of the fairing at approximately 55 ft/s. The velocity of the air then continues to decrease until the trailing edge of the fairing. The air is slowed down to approximately 30 ft/s at the end because of flow separation due to an unfavorable pressure gradient.

Manufacturing

One of the most important factors in the design of the vehicle is the restraint caused by the budget. The 5000 dollar budget will be used for purchased parts, material and manufacturing of the vehicle. The decisions that resulted in the optimal design were heavily influenced by the restriction of the budget. In order to ensure that all the money could be used in the construction of the vehicle the budget was divided in half and shared between the frame and fairing team.

By using off-the-shelf items and donated parts and materials the frame team and fairing team were able to build the vehicle with only 5000 dollars. In reality manufacturing this vehicle would cost more since all parts need to be purchased and labor would not be free. Including all parts purchased, donated, materials and manufacturing the actual cost of the frame and fairing are shown below.

Components Name/Brand/Description	Cost in Dollars	Quanity	Price
Rouleur carbon GXP 53/39 with BB	300.00	1	300.00
(Bottom bracket w/t cerramic bearings) fsa k-force megaexo 24mm	200.00	1	200.00
Carbon Seat Shell	225.75	1	225.75
Avid 07 Juicy 7 160mm Rr w/RH lever Gray/Silver	151.00	2	302.00
look keo clip on pedals (set)	80.00	1	80.00
pyramid Rear Derailleur with hanger clip	7.00	1	7.00
catrike Idler Kit	133.40	1	133.40
ZS-2 Headset includes cups, bearings, crown race, & dust cover	45.00	2	90.00
Handlebar grips	10.00	1	10.00
Squeez Water Bottles locomotion	1.99	1	1.99
xlab carbon cage	33.00	1	33.00
Polar CS200 Bike Compute	23.99	1	23.99
Front Bar-end Shifter	80.00	1	80.00
Front Derailleur	35.00	1	35.00
18" Front wheels (355mm)	80.00	2	160.00
Front Wheel Axles (pair)	45.00	2	90.00
Steering Spindles (pair)	45.00	2	90.00
External Boom 1.75" OD with bottom braket tap	85.00	1	85.00
Handlebars (pair)	29.99	2	59.98
Chain	45.00	1	45.00
Nexus Hub	310.00	1	310.00
Quick Release Salsa seat clips Salsa	8.00	2	16.00
Nexus Hub Shifter/Cables	24.95	2	49.90
Aluminum Rodends	10.00	2	20.00
Manufacturing and Materials	800.00	1	800.00
Total in dollars	**N/A**	**N/A**	**3248.01**

Figure 3.10 Actual cost of building one frame

In order to build one frame it would cost 3,248 dollars. Increasing the production of the frame would decrease the price since material would be purchased in bulk and manufacturing would be optimized. It should also be noted that these costs did not involve the team's time and effort spent on the It would cost approximately 2,800 dollars to manufacture 100 frames, and 2,200 dollars to manufacture 1,000 frames.

The fairing cost 2489 dollars to construct. Since about half of the fairing budget was used to create the plug and negative, when constructing a replica only material would need to be purchased.

	One Fairing	100 Fairing	1000 Fairings
Plug and Negative Mol	$1,200	0	0
Materials	$1,289	$800	$500

Figure 3.11 Cost of building the fairing

Since about half the budget was used to build the plug and negative mold it would be much cheaper to construct multiple fairings. Manufacturing 100 fairings would approximately cost 800 dollars and 1000 dollars to manufacture 500 dollars.

Testing

During a year long project such as the construction of a Human Powered Vehicle (HPV), it is crucial that additional testing be performed. These tests include comparing Computational Fluid Dynamics (CFD) results with actual measurements. Regardless of what additional testing is performed, it supplies the engineer with valuable data that can improve the performance or safety of the vehicle. The fairing team performed several wind tunnel tests during the construction of the HPV.

Wind Tunnel Testing

Wind tunnel testing is one of the most useful and advantageous tools used in industry for aerodynamic study. The information obtained from a wind tunnel is mainly aerodynamic pressures and forces that correlate to the amount of drag or lift experienced on the object. Wind tunnel testing in industry

makes wide use of these experimental measurements. These models provide useful information that can translate to a much larger model. The price to perform wind tunnel testing on a small scale model is significantly lower than actual testing on the full scale model. Therefore, small scale wind tunnel testing provides an alternative for cheap and accurate measurements.

Most of the experiments performed in wind tunnels are common shapes that have been extensively studied. These common shapes provide useful information for engineers in order to grasp aerodynamic theory. When testing an actual small scale aerodynamic body, the results are unique characteristics and measurements that represent that specific model. A picture of the scaled version of the fairing is shown in Figure 4.1. By successfully modeling the small scale model with Computational Fluid Dynamics (CFD), the results can be verified and information can be gained about the design.

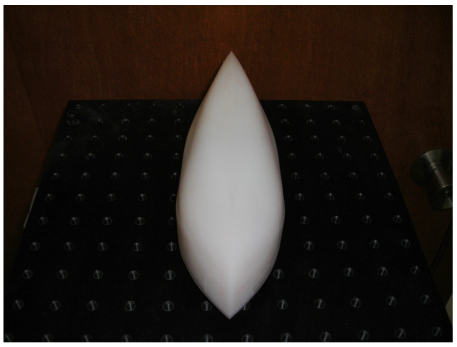

Fig. 4.1a Fairing model

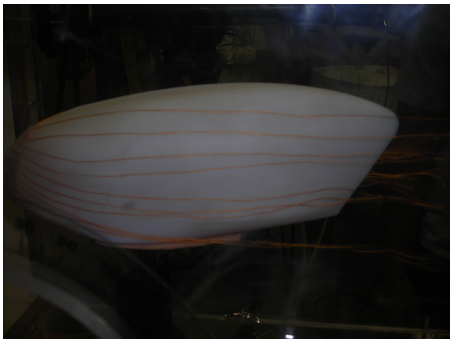

Figure 4.1b Flow string test

One of the first experiments performed was attaching strings to the front of the vehicle and observing the flow across the fairing's aerodynamic body, shown in Figure 4.1b. This will allow the engineer to grasp the pressure gradient across the body and its effect at the point of flow separation. On the model, flow separation occurred approximately one inch from the end of the fairing which represents one foot on the full scale fairing. The coefficient of drag was measured by attaching the model to a lift/drag stand. Drag is the component of force on a body acting parallel to the direction of relative motion. The result of this test was verified by the CFD performed on the model and shown in Table 4.1 below.

Method	Results (Cd)
Wind Tunnel	0.1604
Cosmos CFD	0.25

Table 4.1 Comparison of CD's

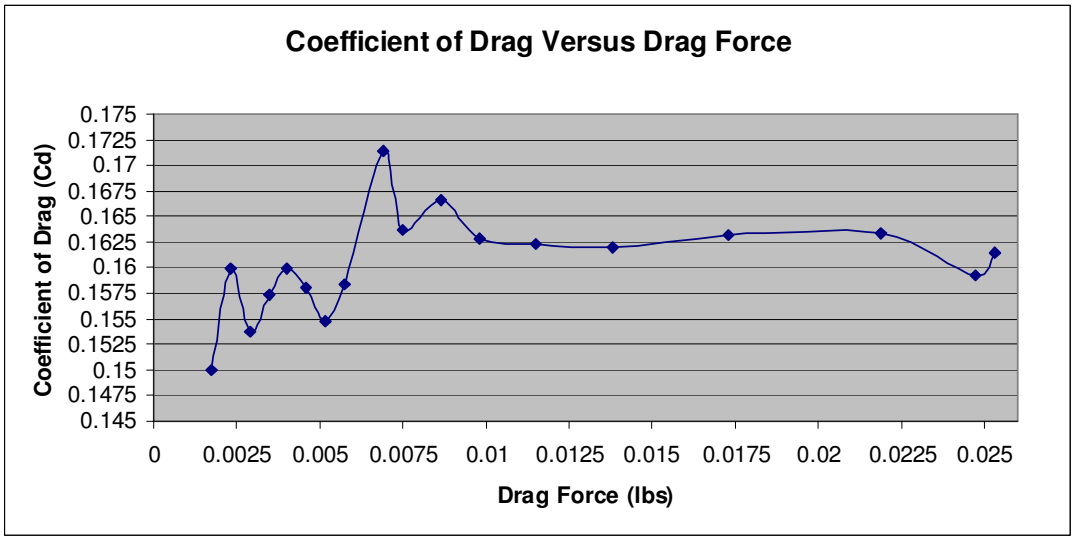

Figure 4.2 Graph of coefficient of drag versus drag force

Plotting the coefficient of drag versus drag force is shown in Figure 4.2. The general shape of the graph resembles an upside down wide parabola, which agrees with aerodynamic theory.

Holes were drilled along the top and side of the body and metal rods inserted inside the holes. The metal rods were also attached to rubber hoses, shown in Figure 4.3a and 4.3b. When the rubber hoses are connected to a pressure transducer, pressures can be obtained across the top and side of the model. This test quantifies the change of static pressure across the body.

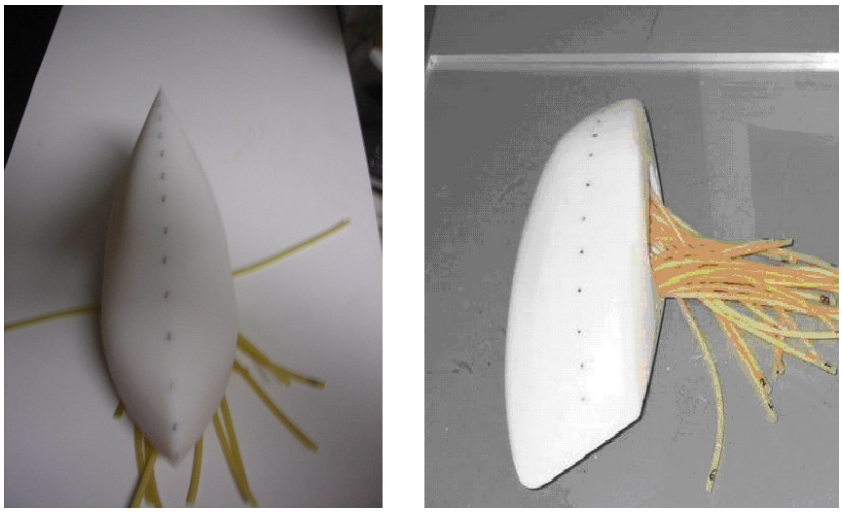

Figure 4.3a,b Top and side view of pressure taps

Inserting the model in the wind tunnel and measuring each pressure tap in the transducer the static pressure can be recorded across the fairing model. Static pressure measurements will be measured in order to quantify when flow separation occurs. The dynamic pressure inside the wind tunnel was measured to be 2.03 inches of H2O, which represents a flow speed inside the tunnel of 64.12 mi/hr. The flow velocity was maintained constant throughout the testing. The static pressure across the top of the fairing is shown in Figure 4.4.

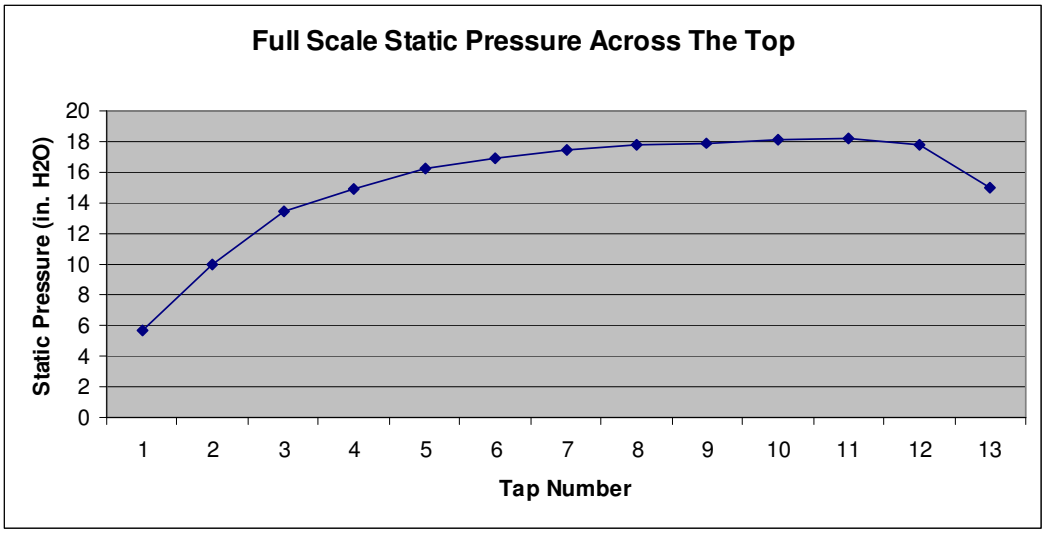

Figure 4.4 Static pressure across the top of the fairing model

The above graph shows that the static pressure increases across the top until the last two pressure taps. Flow separation approximately occurred 1.25 inches from the model representing 1 foot 3 inches on the full scale model. Similarly the static pressure across the side of the fairing model is shown in Figure 4.5.

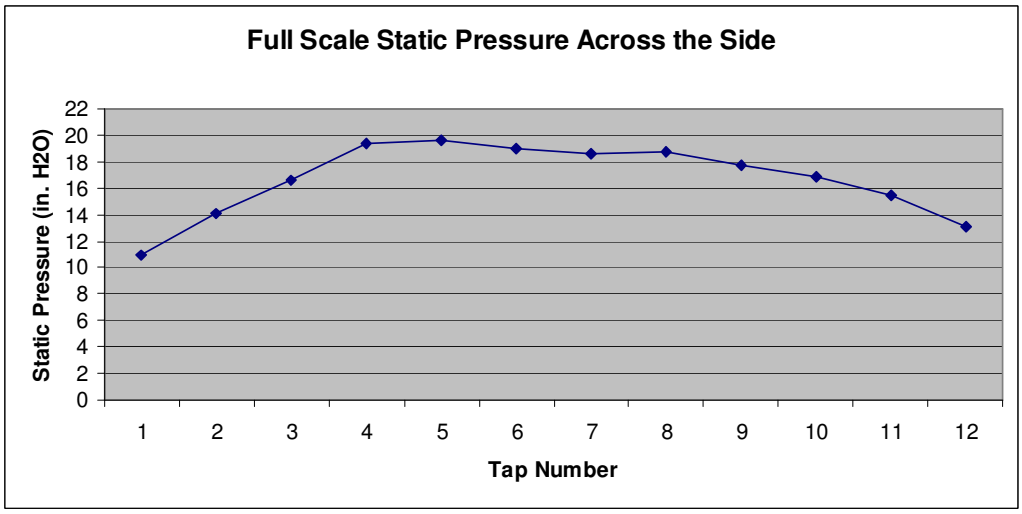

Figure 4.5 Static pressure across the side of the fairing model

The above graph shows that the static pressure increases across the side of the model and then it remains constant until the last four pressure taps. Flow separation approximately occurred 1 inch from the model representing one foot on the full scale model.

The wind tunnel tests successfully helped the team understand how the fairing performs. The flow string test visually portrays how the flow stays attached until one foot from the full scale model. The fairing design has been optimized in order to decrease the distance of this separation from the trailing edge. The design of the fairing resembles and performs like the optimized streamlined aerodynamic body that was desired. The static pressure analysis that was performed aided in understanding the change of pressure across the fairing. At the front of the fairing, the stagnation point, the pressure was low as it increased across the body. The static pressure should increase until the flow begins to separate which causes the static pressure to decrease. The body of the fairing has been optimized in order to reduce the affect of flow separation.

Work Cited List

Stanek, Alex, "Proper Bicycle Fit Explained", Smart Cycles Inc, Sept. 10. 2005, Aug. 20. 2006, http://www.smartcycles.com/fitting_explained.htm

Emmet A. Mossman, Lauros M. Randall, "An Experimental Investigation of the Design Variables for a NACA Submerged Duct Entrance", National Advisory Committee for Aeronautics, Jan. 8. 1948, Nov. 11. 2006, http://naca.central.cranfield.ac.uk/reports/1948/naca-rm-a7i30.pdf

Wichers Schreue, Ben, "The Ventilation of a Streamlined Human Powered Vehicles", Abbot and Wilson, June. 28. 2004, Nov. 13.2006, http://www.hupi.org/HPeJ/0002/ventilation2.pdf

Katz, Joseph, Ph.D, Race Car Aerodynamics, Cambridge Ma: Bentley Publisher, 2007

Johson, Sandra, "Orlando Weather", City rating, January.11. 2007, March. 01. 2007, http://www.cityrating.com/averagetemperature.asp